Defence Research and Development Canada
Recherche et développement pour la défense Canada

CAN UNCLASSIFIED

DRDC | RDDC
technologyscienceetechnologie

Antenna RCS Characterization using SEM approach

Abdelelah M. Alzahed
Said M. Mikki
RMCC-Royal Military College of Canada

Yahia M. M. Antar
UNH-University of New Haven

Prepared by:
Royal Military College of Canada
P.O. Box 17000, Stn. Forces
Kingston, ON, Canada K7K 7B4
Contract Project Manager: Xuemin Wang, 613-949-0557
Contract Number: SLA RMCC-DRDC Serial #2014-007-SLA, Annex #PA14006 - SEM Development for Antenna Characterization

Technical Authority:
Michel Clénet Scientist
Slobodan Jovic, Engineer
(DRDC – Ottawa Research Centre)
Contractor's date of publication: December 2017

Defence Research and Development Canada
Contract Report
DRDC-RDDC-2017-C335
October 2018

CAN UNCLASSIFIED

Canada

IMPORTANT INFORMATIVE STATEMENTS

This document was reviewed for Controlled Goods by DRDC using the Schedule to the *Defence Production Act*.

Disclaimer: This document is not published by the Editorial Office of Defence Research and Development Canada, an agency of the Department of National Defence of Canada but is to be catalogued in the Canadian Defence Information System (CANDIS), the national repository for Defence S&T documents. Her Majesty the Queen in Right of Canada (Department of National Defence) makes no representations or warranties, expressed or implied, of any kind whatsoever, and assumes no liability for the accuracy, reliability, completeness, currency or usefulness of any information, product, process or material included in this document. Nothing in this document should be interpreted as an endorsement for the specific use of any tool, technique or process examined in it. Any reliance on, or use of, any information, product, process ormaterial included in this document is at the sole risk of the person so using it or relying on it. Canada does not assume any liability in respect of any damages or losses arising out of or in connection with the use of, or reliance on, any information, product, process or material included in this document.

© Her Majesty the Queen in Right of Canada, Department of National Defence, 2017

© Sa Majesté la Reine en droit du Canada, Ministère de la Défense nationale, 2017

Abstract

The report investigates antenna characterization using the singularity expansion method (SEM) in both time and spatial-frequency domains. The motivation is to obtain the radar cross section (RCS) of targets through newly and efficient methods. The investigation covers three target types; dipole (thin-wire), u-strip patch and helical antennas. Each target's features are determined using the temporal SEM approach and also by the newly developed approach antenna current Green's function (ACGF) in spatial-frequency domain. The temporal SEM works by inspecting the time domain field representation within a specific time window. In contrast, the ACGF approach is applied on the targets characteristic current (surface current due to special excitation). Both methods are applied on the three mentioned targets to validate the concept.

Résumé

Le rapport étudie la caractérisation d'antenne en utilisant la méthode d'expansion de la singularité (SEM) dans les domaines temporels et spatiotemporels. La motivation est d'obtenir la section efficace du radar (RCS) des cibles grace a des méthodes nouvelles et efficaces. L'enquete couvre trois types de cibles ; dipole (fil mince), patch en U et antennes hélicoidales. Les caractéristiques de chaque cible sont déterminées a l'aide de l'approche temporelle SEM et aussi par la fonction de Green de l'antenne d'approche nouvellement développée (ACGF) dans le domaine spatial-fréquence. Le SEM temporel fonctionne en inspectant la représentation du champ du domaine temporel dans une fenetre temporelle spécifique. En revanche, l'approche ACGF est appliquée sur le courant caractéristique des cibles (courant de surface du a une excitation spéciale). Les deux méthodes sont appliquées sur les trois cibles mentionnées pour valider le concept.

This page intentionally left blank.

Table of contents

Abstract i

Résumé i

Table of contents iii

List of figures v

List of tables viii

1 Introduction 1

1.1 Background 1

1.2 Theory 1

1.3 Singularity Expansion Method (SEM) 2

1.4 ACGF Fundamental definition 3

1.5 SEM-classical modeling Vs ACGF-SEM 5

1.6 Radar Cross Section 6

1.7 RCS-ACGF-SEM 7

2 Thin-wire experiment 8

2.1 Time domain SEM approach 10

2.2 Spatial-frequency ACGF-SEM approach 13

3 Patch Antenna 14

3.1 Time domain SEM approach 18

3.2 Spatial-frequency ACGF-SEM approach 20

4 Helix antenna 24

4.1 Time domain SEM approach 27

4.2 Spatial-frequency ACGF-SEM approach 29

5 Conclusion 32

Annex A: MATLAB codes 33

References 43

List of figures

Figure 1: Target detection scenario by using SEM classical approach 3

Figure 2: Combined general description of antenna system 5

Figure 3: Concept of Radar Cross Section (RCS) 6

Figure 4: RCS for sphere of radius 'a' 7

Figure 5: Dipole antenna layout in EM simulation 8

Figure 6: Dipole antenna frequency dependent RCS 9

Figure 7: The reflection coefficient expressed in (dB) for dipole antenna operating around 1.9 GHz 9

Figure 8: The reflection coefficient expressed in (dB) for dipole antenna operating around 2.4 GHz 10

Figure 9: Plane wave excitation of thin-wire dipole scatterer operating at 1 GHz. 10

Figure 10: Time domain electric field of thin-wire dipole scatterer working at 1 GHz. 11

Figure 11: SEM fitting of time domain field of thin-wire dipole scatterer. . . 12

Figure 12: Thin-wire dipole SEM complex poles representation. 12

Figure 13: The validation of ACGF Vs ACGF-SEM to represent the antenna surface current at different elevation angles: receiving mode operation 13

Figure 14: SEM spatial representation plot; poles are represented as "X" while the residues are represented as "O". Only two poles and residues are required to reconstruct the ACGF data 14

Figure 15: Microsrip square patch antenna: 3D schematic and probe-feed . . 15

Figure 16: The reflection coefficient expressed in (dB) for patch antenna operating around 1.9 GHz 15

Figure 17: The reflection coefficient expressed in (dB) for patch antenna operating around 2.4 GHz 16

Figure 18: Microstrip patch antenna frequency dependent RCS 16

Figure 19: Microstrip patch antenna RCS back scattered field simulated results; Polar representation 17

Figure 20: Microstrip patch antenna RCS back scattered field simulated results; 3D representation 17

Figure 21: Plane wave excitation of u-strip patch in scattering mode at 1.9 GHz. 18

Figure 22: Time domain electric field in x-direction of u-strip patch in scattering mode at 1.9 GHz. 19

Figure 23: SEM fitting of time domain field in x-direction of u-strip patch in scattering mode. 19

Figure 24: SEM complex poles representation of u-strip patch in scattering mode. 20

Figure 25: Microstrip patch antenna current distribution: 3D representation . 21

Figure 26: Microstrip patch antenna meshing grid in ADS MoM solver 21

Figure 27: Microstrip patch antenna surface current along its width from ADS MoM solver 22

Figure 28: SEM spatial poles representations of microstrip patch antenna, the optimized poles are represented as “X” while the approximated approach is showing TWO poles on each cell 23

Figure 29: Microstrip patch antenna reconstructed surface current given from optimizing the SEM poles and residues 23

Figure 30: Helix antenna and dimensions 24

Figure 31: Return loss in (dB) of Helix antenna operating between 1.6 to 2.4 GHz 25

Figure 32: Helix antenna frequency dependent RCS 25

Figure 33: Helix antenna radiation pattern in normal mode (Broadside); 3D representation 26

Figure 34: Helix antenna radiation pattern in axial mode (end-fire); 3D representation 26

Figure 35: Plane wave excitation of Helix in scattering mode between 1 to 2.4 GHz. 27

Figure 36: Time domain electric field in z-direction of Helix in scattering mode between 1 to 2.4 GHz. 28

Figure 37: SEM fitting of time domain field in z-direction of Helix in scattering mode. 28

Figure 38: SEM complex poles representation of Helix in scattering mode. . . 29

Figure 39: Helix antenna current distribution; 3D representation 30

Figure 40: Helix antenna current distribution; 2D representation 30

Figure 41: ACGF Vs ACGF-SEM of helix antenna 31

Figure 42: SEM poles representation of helix antenna 31

List of tables

Table 1: Dipole antenna dimensions 9

Table 2: Patch antenna dimensions 15

Table 3: SEM spatial poles representation of microstrip patch antenna cells 22

Table 4: Helix antenna design dimensions 24

1 Introduction

1.1 Background

Antennas can be characterized using various parameters such as gain, radiation properties and their cross sectional area [1]. These parameters can be expressed at a single operating frequency in order to obtain a single mode system, which is created by probing the antenna by a definite voltage signal, or a time domain approach that shows a wide spectral data that also requires a short impulse to be injected to the antenna. Time domain approaches are preferred for ultra wide band and high speed applications, however, this imposes a difficulty in determining the antenna's characteristics due to the random perturbations of time domain signals and noise. On the other hand, frequency domain approaches are preferred in high power systems because of the possibility of suppressing the noise without affecting the primary signal. In this report, we are going to characterize different targets specifically dipole, u-strip patch and helical antennas in both time domain and spatial-frequency domain approaches by showing their radiation characteristics and RCS properties.

1.2 Theory

The motivation behind this work is to investigate the SEM in spatial domain using the ACGF spatial function. The reason for that is to maintain a complete understanding of how the SEM radar system works. It was observed from the classical SEM that one can detect targets from the echo signal generated when hitting the target with a plane wave which was technically proved. However, the SEM method stated clearly that not all the echo signal is representing the target response but part of it called the late response. The late response is captured experimentally by excluding the time in which a signal travels to a target and reflects back and thus the remaining part is considered the target response. The late response represented in time domain is then transformed to frequency domain by obtaining poles and residues. Obviously, this is not a rigorous approach due to the inaccurate estimation of the signal's travel time. Moreover, the receiver module task is crucial that requires to allocate a large memory and signal processing units. The proposed concept is to modify the SEM model to interpret the resulted echo signal but on the target side. This is done by obtaining the ACGF which is used to determine the target's far field response as well as near field. The ACGF is a spatial function defined on the target's surface as will be illustrated later, so, it shows the target's response to a plane wave and hence it is possible to maintain the echo signal by performing Green's integral along the target's surface to find the late response. This approach will work with the classical SEM approach to reduce the calculation complexity where the system works as follows, first the radar system captures the echo signal represented as the time domain electric field that includes the target response with other scattered fields, at the same time the ACGF field will work in parallel to the first process and

evaluates the system field. However, the ACGF requires prior knowledge of the system which can be acquired by EM simulators. At the end, the two fields, i.e. from the radar system and ACGF, are then correlated together at the receiver end in order to distinguish the target type. The final detection is performed by correlating the received signal with many ACGF fields each is representing a certain target. The new system provides an accurate detection compared with the classical one, however, it presume the realization of ACGF for each expected target. The new approach will be investigated through many examples at different operating frequencies. Each example involves and shows ACGF defined on single and multi-dimensional surfaces. The final step is to verify the proposed approach by comparing the resulted echo from ACGF-SEM method with measured data using the facility in the Royal Military College of Canada.

1.3 Singularity Expansion Method (SEM)

Since it is proposed many decades ago, the Singularity Expansion Method (SEM) [2] has enjoyed a tremendous popularity in both computational and applied electromagnetics due to its very generic character and numerical robustness. For example, it was applied to target identification [3] and numerous other antennas and scattering scenarios (see the survey [4] for more references and discussion). The existing SEM, however, is essentially a time-domain approach where a temporal signal, say the measured radar echo, is probed in order to determine its deeper spectral composition, namely the time signal's poles and their residues. Moreover, the SEM approach introduces a simple representation of the system by a finite number of data, complex poles and residues. Furthermore, the mathematical representation of SEM is similar to the basic Laplace transformation when representing the system in the frequency domain as shown in [2]. In fact, Carl B. mentioned in [2] the fundamental differences between the SEM and the Laplacian model in building the mathematical expression that links the time signal to frequency representation. As for target detection and radar systems, the SEM can be an efficient approach to deal with targets in time domain due to some important factors listed as follows;

1. Incident wave angle independent
2. Excitation signal independent
3. Polarization independent

The system works as shown in Figure 1 by processing the return field echo and split it into two prominent time intervals; the first is called the early time response, which appears as a result of impinging the incident signal on the target and the latter is the late time response that represents the target unique response that comes after the early response interval. Both early and late times are an estimation of the time

that the incident signal takes to complete a full transceive cycle, i.e. starting from Tx antenna and reflected back from the target to reach Rx terminal. It is shown in [3] that SEM method only deals with an invariant quantity that represents the target response regardless of any changes in the environment. From a different perspective, SEM can be interpreted as the target response due to an impulse excitation, where the incident signal hits the target causing a surface current to flow that also results in a late radiation corresponding to this current. Moreover, the current shaped according to the natural resonance of a target. For example, if we assumed a time-domain delta source excitation, in which for a thin-wire antenna the surface current forms a half wavelength in terms of the operating frequency. In other words, the target filters the frequencies from the incoming impulse signal into a single frequency which is a function of its spatial properties. As a result, it is required to restrict SEM to only model the target's late response that represents the antenna impulse response (AIR) in time domain.

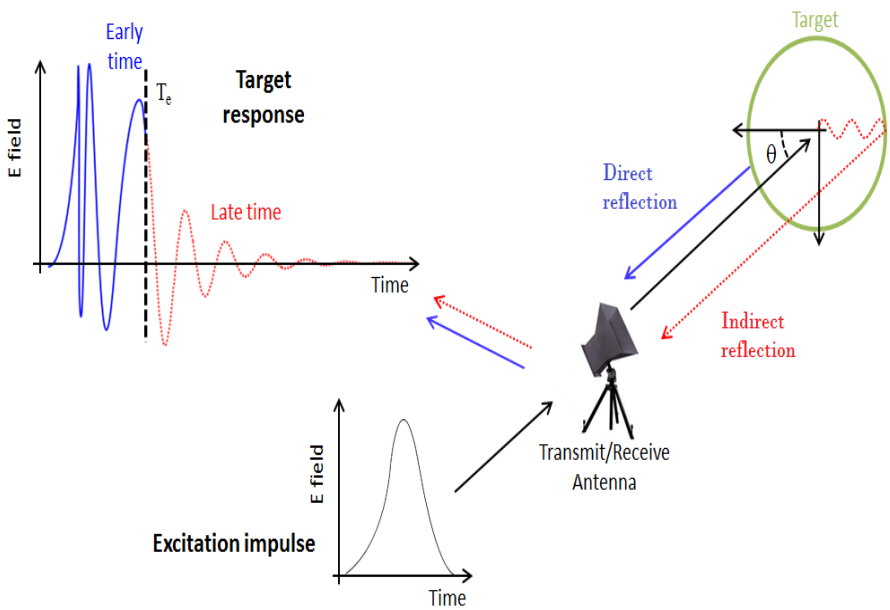

Figure 1: *Target detection scenario by using SEM classical approach*

1.4 ACGF Fundamental definition

We consider a thin-wire antenna supporting a current $\mathbf{J}(\mathbf{r}, t)$ radiating in infinite and homogeneous free space medium with dielectric permittivity ε_0 and magnetic permeability μ_0. The antenna is oriented along the direction of the vector $\mathbf{L}$ where L is the total length. A time harmonic excitation $\exp(-i\omega t)$ is assumed and suppressed everywhere. The frequency-domain ACGF [5] and [6] of this antenna can be written in the form $\hat{L}\hat{L}\, F(\mathbf{r}, \mathbf{r}'; \omega)$, where $\hat{L} := \mathbf{L}/L$ is a unit length vector in the direction of

the antenna. Formally, the ACGF is defined by the following operator equation

$$F\left(\mathbf{r},\mathbf{r}';\omega\right)=\mathcal{L}^{-1}\left\{\delta_{L}\left(\mathbf{r},\mathbf{r}'\right)\right\}. \tag{1}$$

Here, $\mathcal{L}$ is the electromagnetic operator of the antenna connecting the (tangential) radiated field E to the surface current J through $E=\mathcal{L}J$. $\delta_{L}\left(\mathbf{r},\mathbf{r}'\right)$ is a special surface delta function tangential to the antenna surface L. The operator inversion (1) leading to the ACGF was shown to be possible in general by actually constructing the ACGF through a sufficiently generic sequential distributional series [7]. In terms of this function, if an arbitrary tangential field excitation $\mathbf{E}_{\text{ex}}\left(\mathbf{r}'\right)=\hat{L}E_{\text{ex}}\left(\mathbf{r}'\right)$ is applied on the antenna $\mathbf{L}$, the excited current is given by [7]

$$\mathbf{J}\left(\mathbf{r}\right)=\hat{L}\int_{L}dl'F\left(\mathbf{r},\mathbf{r}'\right)E_{\text{ex}}\left(\mathbf{r}'\right), \tag{2}$$

where l' serves here as a local length parametrization of $\mathbf{r}'=\mathbf{r}'\left(l'\right)$ along the wire $\mathbf{L}$. The expression (2) is valid for arbitrary tangential field excitations $E_{\text{ex}}\left(\mathbf{r}'\right)$. This is a fundamental difference between obtaining the antenna current $\mathbf{J}\left(\mathbf{r}\right)$ using other numerical methods, say the Method of Moment (MoM). Indeed, in the latter, one has to create a special mesh depending on the wavelength-structure of the excitation field. The ACGF formula (2), however, is valid for *arbitrary* inputs with any wavelength composition as was shown both mathematically and numerically in [7]. It remains true, though, that obtaining such ACGF could be a challenging computational or lab process. To our knowledge, only MoM-approximations of the ACGF has been reported so far. For simplicity, we focus in this paper on ACGFs obtained using a delta-source excitation through an accurate higher order MoM [8]. Experimentally, the ACGF is obtained by enforcing a voltage source with a unit impulse, $V=1Volt$, at a desired location r on the wire surface L. The EM solver is then responsible in generating the meshing grid that segments the surface into N samples. Each sample is defined as a circuit element as in [9] that forms continues circuits along the wire. As a result, it is observed from the EM solver that the system transfer function is given by equation (3)

$$[I]=[Y], \tag{3}$$

Where $[I]$ is the surface current represented on each segment and $[Y]$ is the admittance vector.

In contrast, in MoM program, the generated system output is representing an admittance matrix in which each column is a result of exciting the wire at a different segment (super position excitation). While in our case is re-sampled to the desired port excitation. This approach, however, involves a reciprocal property that links the port voltage/ current value to the system field and vice versa as in Equation 2. The

system in Figure 2 is complete in the sense that the full chain of processes starting from the voltage excitation of a transmitting antenna up to the physical port of a receiving antenna is included in the analysis. We consider the various Green's functions ACGF (current Green's function) and FSGF (free-space Green's function) as exact transfer functions in space.

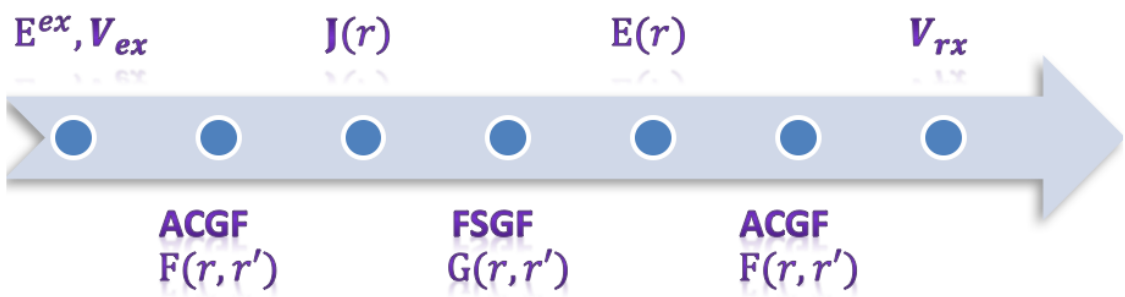

Figure 2: *Combined general description of antenna system*

1.5 SEM-classical modeling Vs ACGF-SEM

The field radiated from an object is defined as in Equation 4, where the surface current density due to an excitation location r' is multiplied by the dyadic Green's function and integrated along the surface or length as the case of wire.

$$\mathbf{E}_{\text{rad}}(\hat{r}) = \int_L dl\, \mathbf{J}(\mathbf{r}') \cdot \left[\bar{\mathbf{I}} - \hat{r}\hat{r}\right] e^{ik\hat{r}\cdot\mathbf{r}'} \tag{4}$$

where $\hat{r}(\theta,\varphi) = \hat{x}\cos\varphi\sin\theta + \hat{y}\sin\varphi\sin\theta + \hat{z}\cos\theta$ is the radial unit vector $\mathbf{r}/\|\mathbf{r}\|$, $\bar{\mathbf{I}}$ is the unit dyad, and $k = \omega/c$, where c is the speed of light.

$$\bar{\mathbf{F}}(\mathbf{r},\mathbf{r}';\omega) = \hat{L}\hat{L}\, F(\mathbf{r},\mathbf{r}';\omega) = \hat{L}\hat{L}\sum_{n=1}^{N} \alpha_n(\omega)\, e^{s_n(\omega)l} + e_N, \tag{5}$$

where here α_n and s_n stands for the SEM *poles strengths* and *poles locations*, respectively. In the familiar temporal SEM [3], the quantities α_n are often denoted *residues*, reflecting their mathematical origin in complex integration theory [10]. We avoid doing so here because, in contrast to the temporal SEM, the quantities α_n defined by (5) can be generalized to 2D current functions, leading to doubly-indexed coefficients α_{mn}, and the latter cannot be traced back to the complex integration theory rooted in 1D functions (time signals.) The quantity e_N appearing in (5) represents the ACGF-SEM error resulting from truncating the series to only N terms. No exact analysis of the behavior of e_N is reported here. Instead, we use brute-force numerical algorithms to obtain the expansion (5) with the smallest possible number of singularities N.

1.6 Radar Cross Section

The RCS of a target can be viewed from Equation 6 as a comparison of the strength of the reflected signal from a target to the reflected signal from a perfectly smooth sphere of cross sectional area of $1m^2$ as shown in Figure 3. In other words, the RCS is the hypothetical area that would intercept the incident power at the target, which if scattered isotopically, would produce the same echo power at the radar as the actual target.

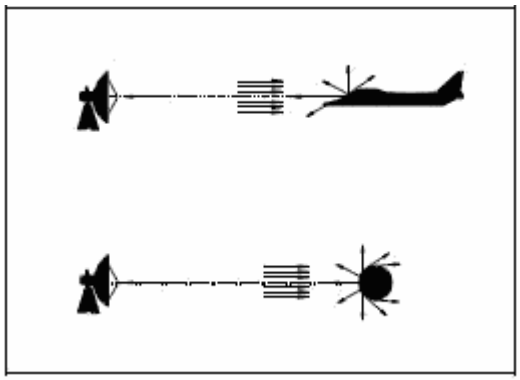

Figure 3: *Concept of Radar Cross Section (RCS)*

$$RCS = \sigma = 4\pi R^2 \frac{\mid E_s \mid^2}{\mid E_i \mid^2} \tag{6}$$

Where R is the radius of the sphere, and E_s and E_i are the scattered and incident electric field, respectively. When a target has very small physical dimensions compared to the wavelength of the incident wave, it is considered that your analysis is being done in the so-called Rayleigh region [11]. In this region, the shape of the object does not influence in determining their RCS, and for some types of objects the RCS is determined from the volume, instead of considering the dimensions and physical forms. For targets that are comparable in size to the wavelength of incident wave, the RCS varies depending on the frequency and is called the resonant region or Mie region. When the dimensions of the target are large compared with the wavelength of incident wave, the RCS can be determined using the methodology of geometrical optics or by the method of optical physics, and this region is called the optical region as in Figure 4. It is observed from the simulated results that the system resonance frequency is located at the maximum peak between Rayleigh region and Mie region.

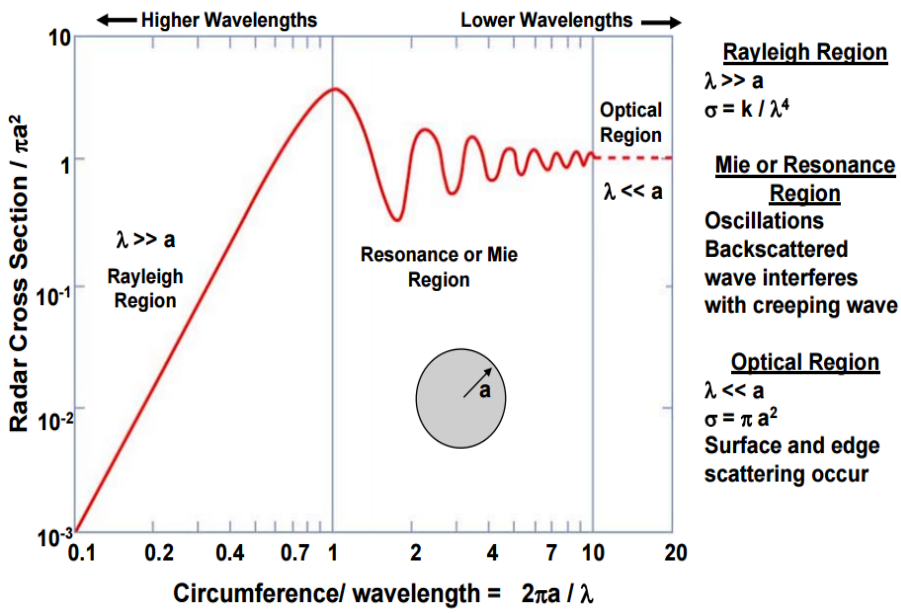

Figure 4: *RCS for sphere of radius 'a'*

It is required to define the most significant parameters in characterizing targets; as a result, the physical geometry and exterior features are in first concern, however, the direction of illuminating radar, the transmitter frequency and the material type are also important.

1.7 RCS-ACGF-SEM

It is well-known from the SEM principle that we can express the antenna far-field through poles and residues. Also, the late time far-field echo as mentioned in Figure 1 is a consequence of the induced current distributed on the antenna surface when illuminated by a plane wave, which is also known as the target natural response. As a result, the echo field is now interpreted as a function of a spatial property and hence can be explicitly represented through the system ACGF. Our approach tends to characterize the ACGF data with SEM poles and residues, thus, the system field can be expressed by Equations (7) and (8) where the generation of the new expression is given for number of poles and residues. Furthermore, our new approach expresses the RCS in terms of the ACGF, in which avoids repeating full-wave simulation.

$$\mathbf{E}_{\text{rad}}\left(\hat{r}\right) = \hat{L} \cdot \left[\overline{\mathbf{I}} - \hat{r}\hat{r}\right] \sum_{n=1}^{N} \alpha_n f_n\left(\theta, \phi; \mathbf{L}, s_n\right), \tag{7}$$

where

$$f_n\left(\theta,\phi;\mathbf{L},\mathbf{r}_p\right) := \frac{e^{\left(ik\hat{r}\cdot\hat{L}+s_n\right)L/2} - e^{\left(-ik\hat{r}\cdot\hat{L}+s_n\right)L/2}}{\left(ik\hat{r}\cdot\hat{L}+s_n\right)}. \tag{8}$$

The RCS-ACGF-SEM approach is being investigated on wire antennas for simple conversion and later on planar structures. Through different radiating structures, it is assumed to verify the new approach with respect to real-time measurements and to process the echo signal to obtain the system poles and residues

2 Thin-wire experiment

In this section we obtain SEM characterization for thin-wire antenna operating at 1 GHz by showing the poles and residues in both time and spatial-frequency domains. First, we start by simulating the antenna under test (AUT) using a computer simulation software (CST-MWS [12]) that generates the EM behavior using a time domain solver (FDTD). Following, we repeat the experiment in frequency domain in order to obtain the spectral signature of the antenna by replicating the design in WIPL-D [13], method of moments (MoM) solver. In both solvers, the antenna is operated in transmitting mode and also in scattering mode where the port is shorted or loaded. The transmitting mode setup is shown in Figure 5 where the antenna is symmetric and excited by a discrete source of 50Ω input impedance while also the antenna dimensions are listed in Table 1 as function of the operating frequency. The antenna is simulated at 1 GHz and in 2 GHz where the return loss is plotted at these operating frequencies as shown in Figures 7 and 8 . Also, Figure 6 shows the antenna RCS in mm^2 with respect to the operating frequency.

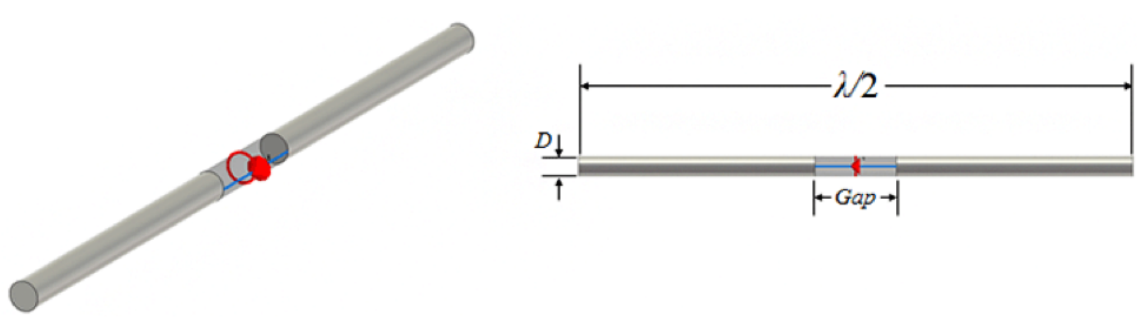

Figure 5: *Dipole antenna layout in EM simulation*

Table 1: *Dipole antenna dimensions*

Dipole length (l)	0.5λ
Port separation (Gap)	0.025λ
Wire radius (D/2)	0.003369λ

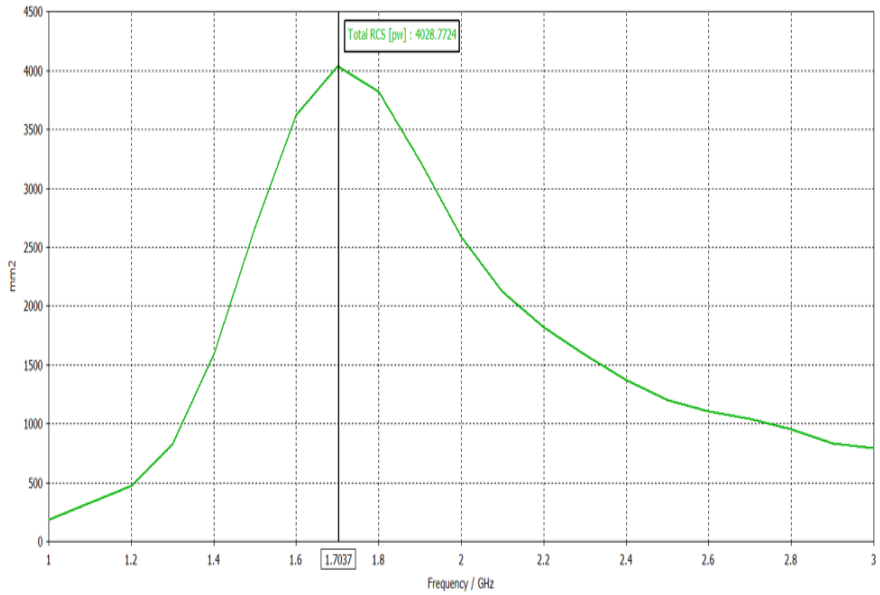

Figure 6: *Dipole antenna frequency dependent RCS*

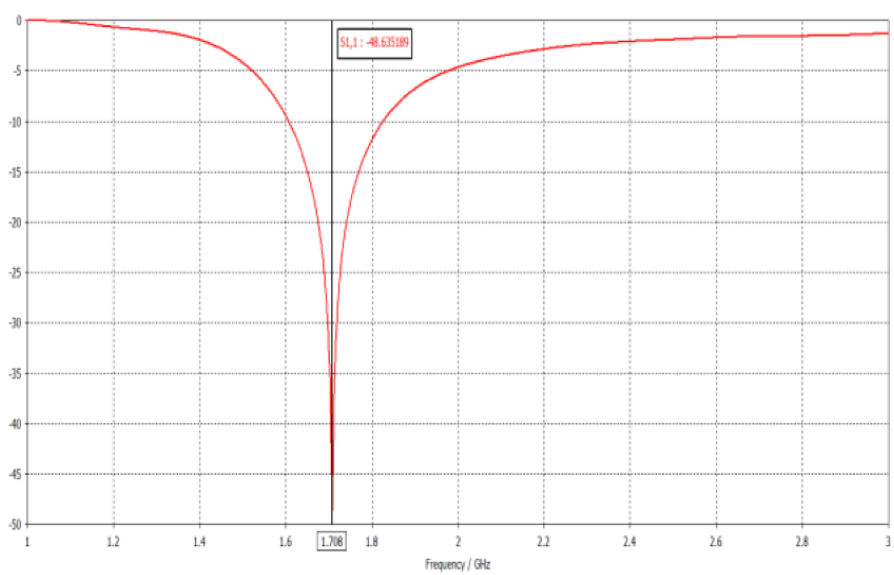

Figure 7: *The reflection coefficient expressed in (dB) for dipole antenna operating around 1.9 GHz*

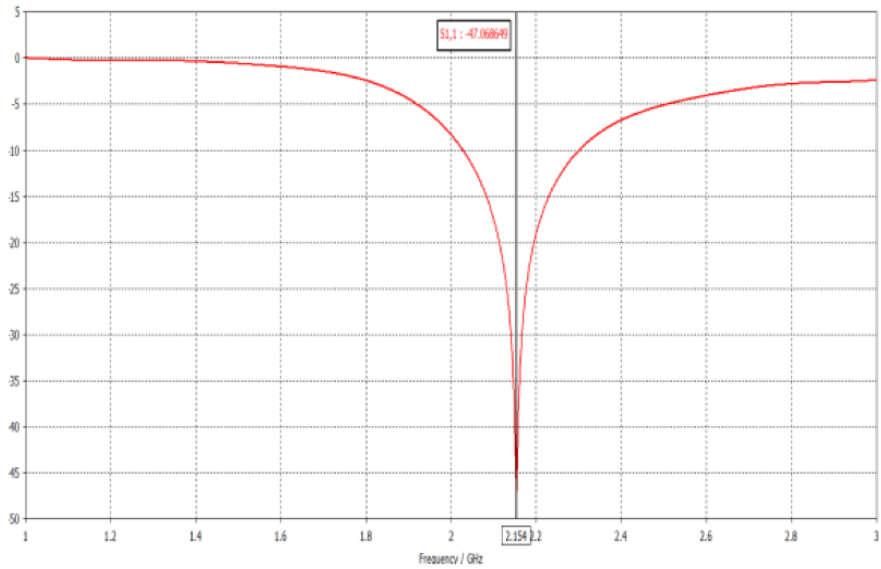

Figure 8: *The reflection coefficient expressed in (dB) for dipole antenna operating around 2.4 GHz*

2.1 Time domain SEM approach

Now, let us consider a scattering scenario where the port is shorted or loaded. A generated plane wave is applied towards the target as shown in Figure 9 where the electric field component is tangential to the element. In CST-MWS, the simulation is performed by modifying the plane wave signal to a unit-impulse as mentioned in SEM literature survey. Also, a field probe is placed between the element and the plane wave source point to capture the scattered field from the element.

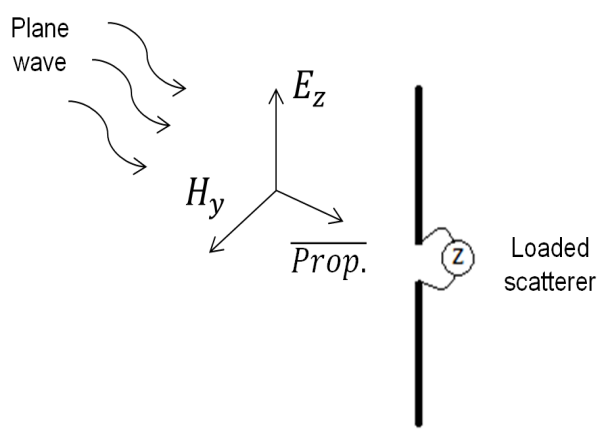

Figure 9: *Plane wave excitation of thin-wire dipole scatterer operating at 1 GHz.*

Figure 10 shows the time domain electric field captured by the inserted probe in the x-direction. It can be observed from the figure the triggered unit-impulse occurring in the beginning, which is also known as the early time response. In SEM modeling, this part is going to be excluded where we are only considering the late time window. In Figure 11, the early time response is truncated leaving only the late time window that is going to be fitted using Prony's method in order to generate the complex SEM poles and residues representation.

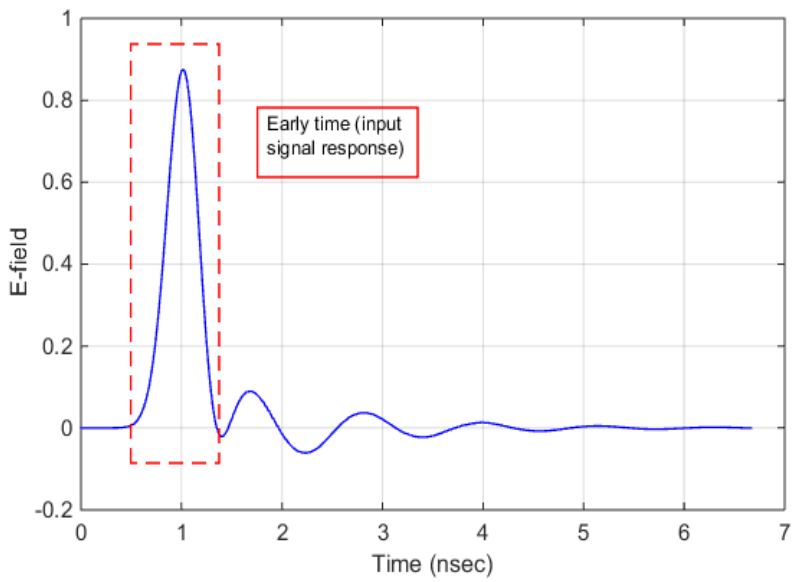

Figure 10: *Time domain electric field of thin-wire dipole scatterer working at 1 GHz.*

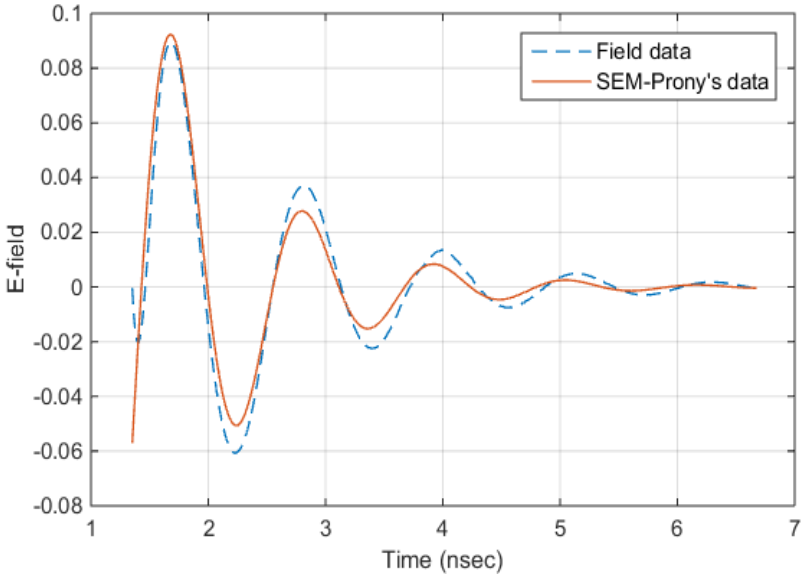

Figure 11: *SEM fitting of time domain field of thin-wire dipole scatterer.*

The complex poles representation of the thin-wire scatterer is presented in Fig.12. It only requires two poles and residues to reconstruct the time domain late time field.

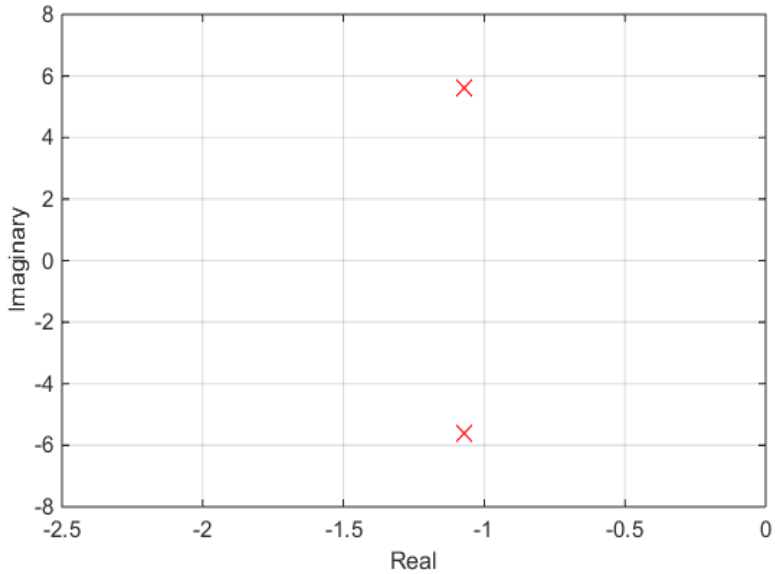

Figure 12: *Thin-wire dipole SEM complex poles representation.*

2.2 Spatial-frequency ACGF-SEM approach

Spatial-frequency approach requires a prior knowledge of the system's transfer function, which is defined earlier as the ACGF. This is done by triggering the element by a unit-delta function on a fixed point of the antenna. This results to the antenna admittance vector as well as the surface current distribution at the same time as in Equation 3. At this stage, the spatial SEM takes place by fitting the generated transfer function using Prony's method as in Equation 9. Through Equation 2 we can determine the received port current that yields to the results shown in Figure 13. Reconstructing the antenna surface current in Equation 9 requires two complex spatial-SEM poles and residues as shown in Figure 14.

$$\overline{F}(r, r^{'}) = \sum_{n=1}^{N} R_n e^{s_n r} \tag{9}$$

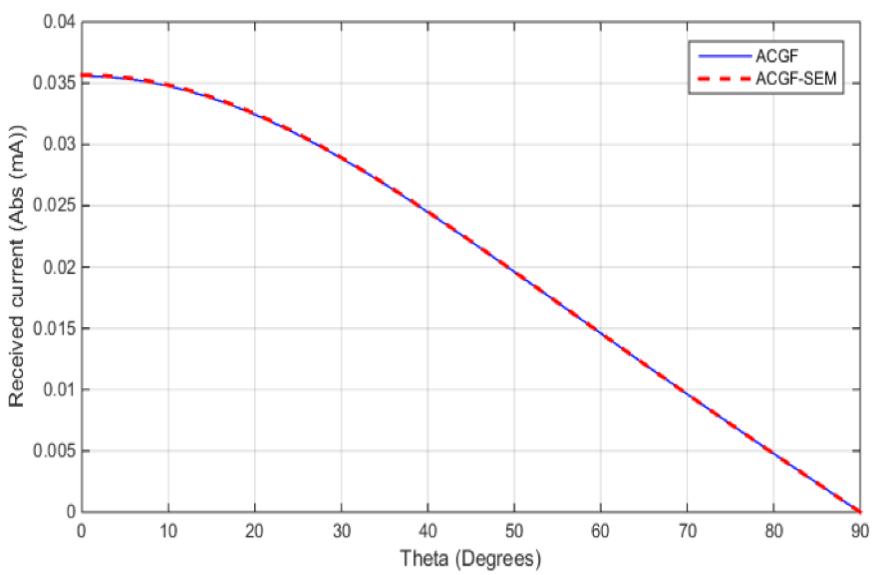

Figure 13: *The validation of ACGF Vs ACGF-SEM to represent the antenna surface current at different elevation angles: receiving mode operation*

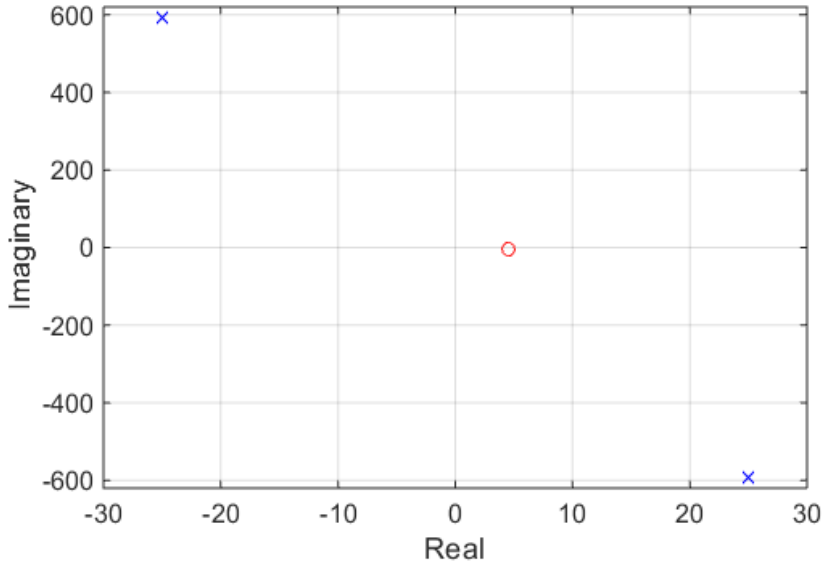

Figure 14: *SEM spatial representation plot; poles are represented as "X" while the residues are represented as "O". Only two poles and residues are required to reconstruct the ACGF data*

3 Patch Antenna

In this section we obtain SEM characterization of u-strip square patch antenna probe fed as shown in Figure 15 operating at frequencies between 1 and 2 GHz by representing SEM complex poles and residues in time and spatial-frequency domains. We simulated the proposed antenna in CST-MWS to obtain time domain data, while the spatial-frequency data were obtained using WIPL-D EM solver. Also, the antenna is simulated in both transmitting and receiving modes in order to obtain its properties as return loss as shown in Figure 16 and Figure 17. The antenna RCS is plotted versus the operating frequency as in Figure 18.

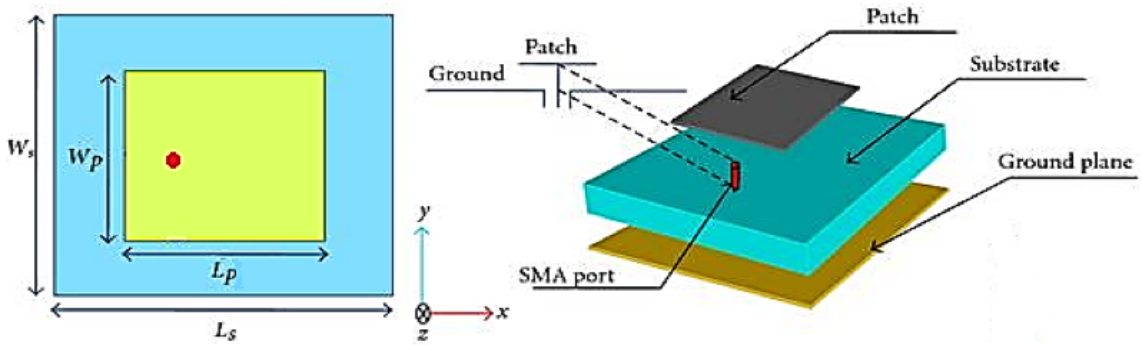

Figure 15: *Microsrip square patch antenna: 3D schematic and probe-feed*

Table 2: *Patch antenna dimensions*

Square pacth at 1.9 GHz	**Square patch at 2.4 GHz**
$L = 37.3335mm$	$L = 29.4431mm$
$W = 48.0458mm$	$W = 38.036mm$
$\epsilon_r = 4.4$	$\epsilon_r = 4.4$
Substrate height $h = 1.6mm$	Substrate height $h = 1.6mm$

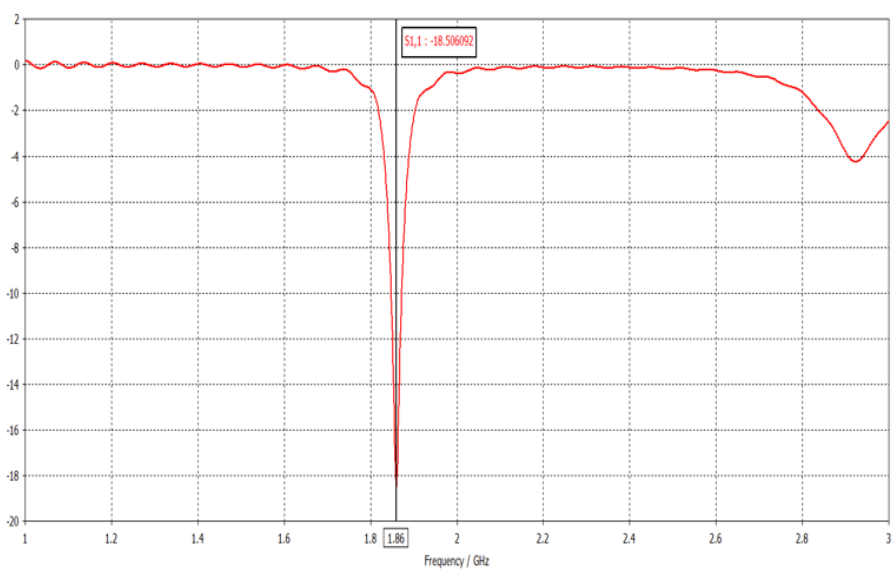

Figure 16: *The reflection coefficient expressed in (dB) for patch antenna operating around 1.9 GHz*

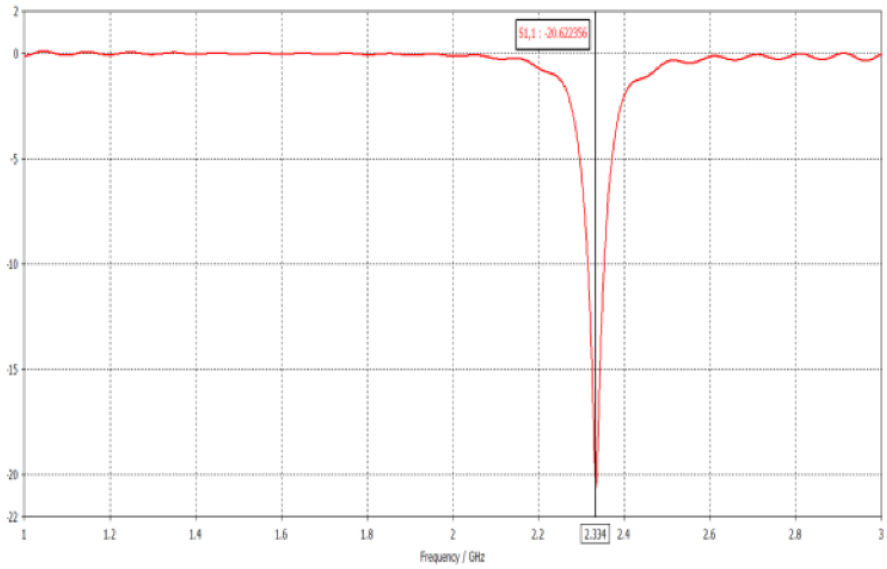

Figure 17: *The reflection coefficient expressed in (dB) for patch antenna operating around 2.4 GHz*

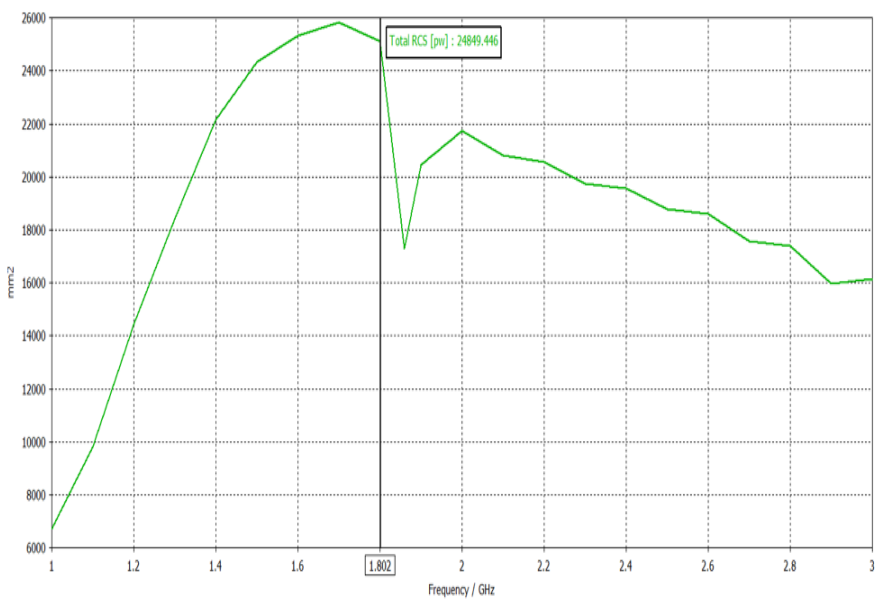

Figure 18: *Microstrip patch antenna frequency dependent RCS*

The backscatered field of the patch is represented in Figures 19 and 20 in polar and 3D pattern, respectively. It can be observed from the plot the effect of the patch's ground when illuminated by a plane wave showing another main lobe on the -ve propagation direction.

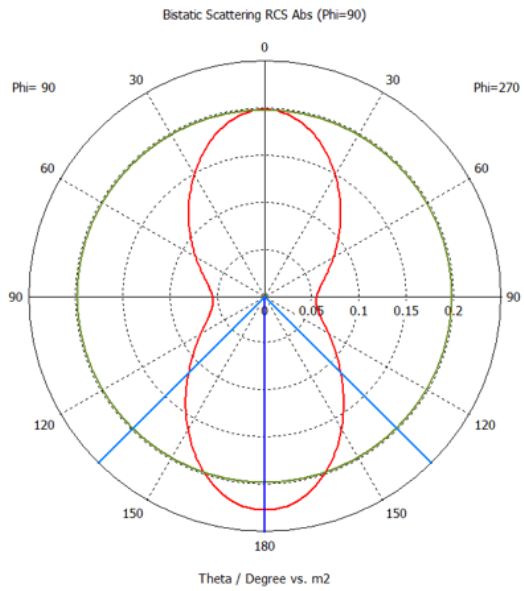

Figure 19: *Microstrip patch antenna RCS back scattered field simulated results; Polar representation*

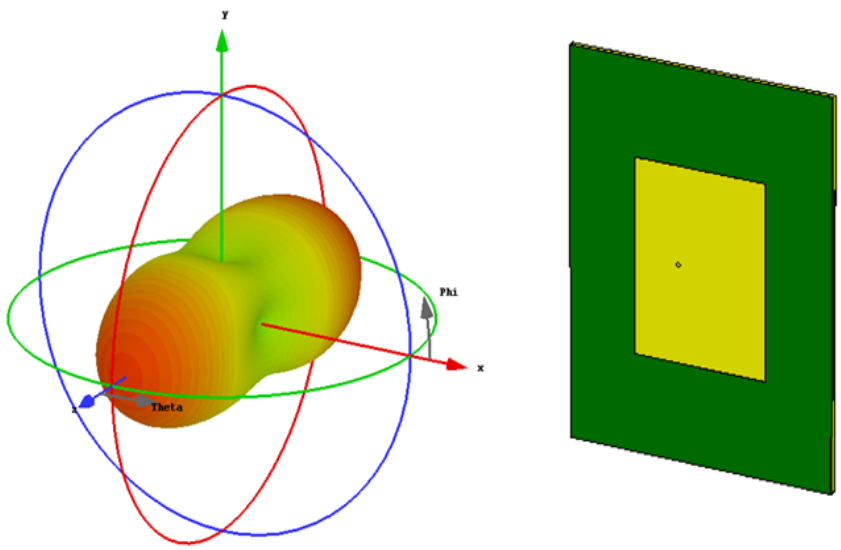

Figure 20: *Microstrip patch antenna RCS back scattered field simulated results; 3D representation*

3.1 Time domain SEM approach

In CST-MWS, a plane wave excitation is assumed to impinge the system as shown in Figure 21, where the electric field component is tangential to the patch surface. Also, the plane wave is assured to be a unit-impulse similar to the previous example. A field probe is placed between the plane wave and the u-strip patch in order to capture the scattered fields from the antenna. The time domain electric field in the x-direction is shown in Figure 22 showing the early time response. The late time response is plotted in Figure 23 in comparison with SEM fitted field using Prony's method where both representation are in close agreement. The complex poles SEM representation is plotted in Figure 24 in which four poles and residues are required to reconstruct the late time field.

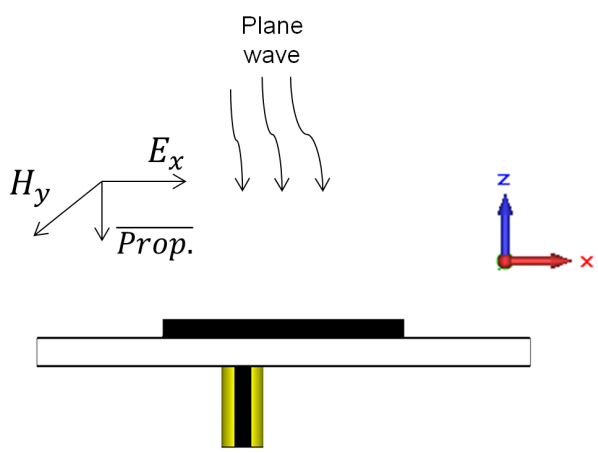

Figure 21: *Plane wave excitation of u-strip patch in scattering mode at 1.9 GHz.*

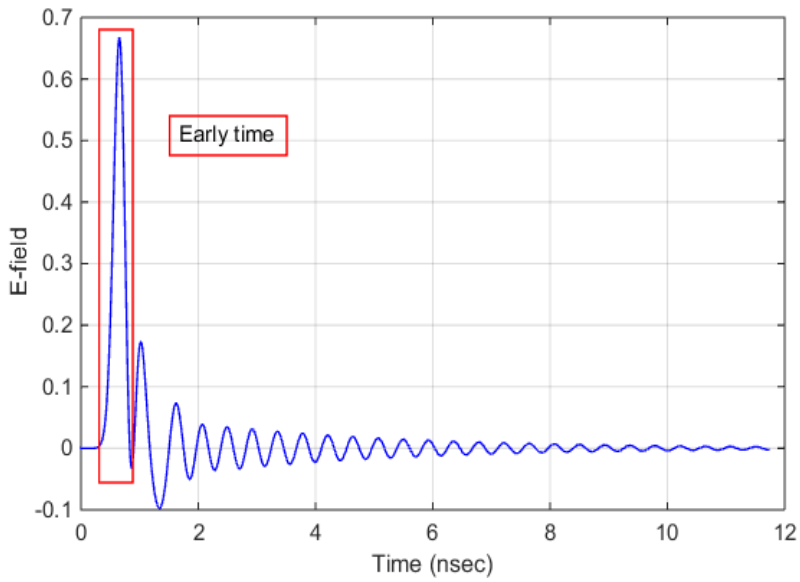

Figure 22: *Time domain electric field in x-direction of u-strip patch in scattering mode at 1.9 GHz.*

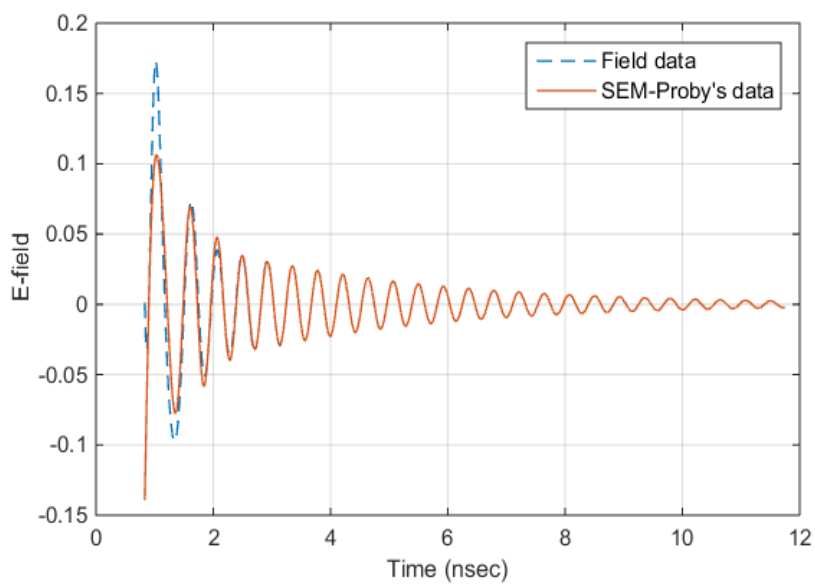

Figure 23: *SEM fitting of time domain field in x-direction of u-strip patch in scattering mode.*

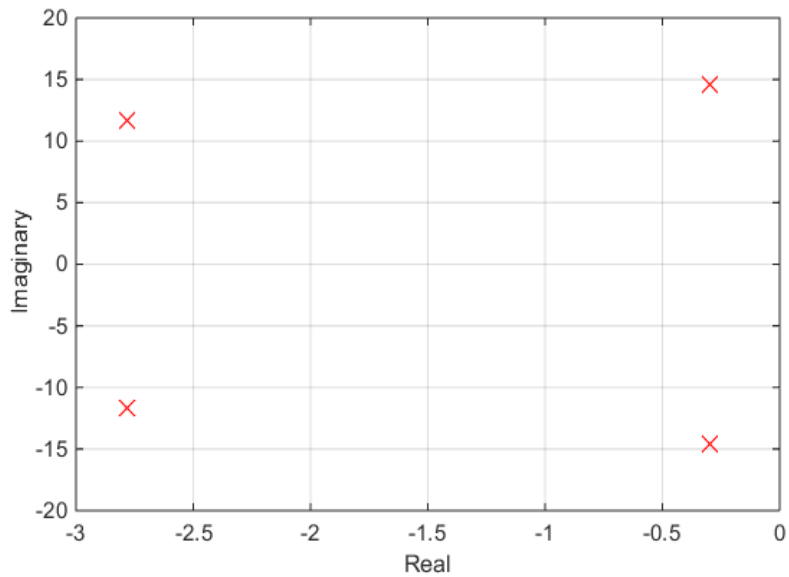

Figure 24: *SEM complex poles representation of u-strip patch in scattering mode.*

3.2 Spatial-frequency ACGF-SEM approach

In order to obtain the spatial-frequency data of the AUT, it is required to generate the ACGF of the system. In the previous example of thin-wire element, the ACGF representation showed a 1D vector of both admittance and surface current. However, in u-strip patch antenna, the ACGF forms a 2D representation as in Figure 25, where the current is defined as two definite components, J_x and J_y. In this section, we are going to approximate the 2D ACGF model into a stacked 1D ACGFs using ADS-EM software [15] as shown in Figure 26 to reduce the calculation complexity of SEM data. In order to mesh the patch's surface, we have to assign a single mode excitation in which is assumed to be the dominant mode TM_{010}. This assumes a significant current perturbations along the patch length and minor variations in its width. Figure 27 shows the minor variations with respect to the patch width, while a half sinusoidal currents form on its length.

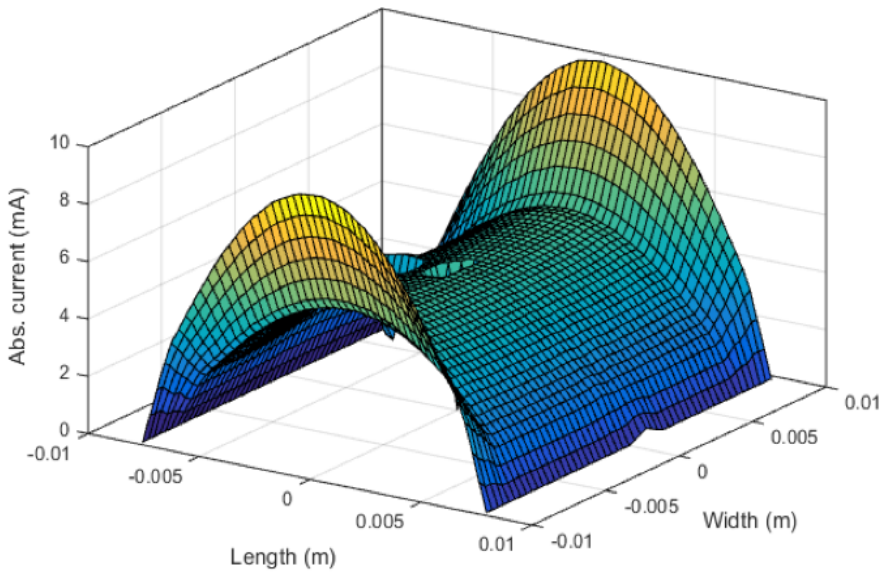

Figure 25: *Microstrip patch antenna current distribution: 3D representation*

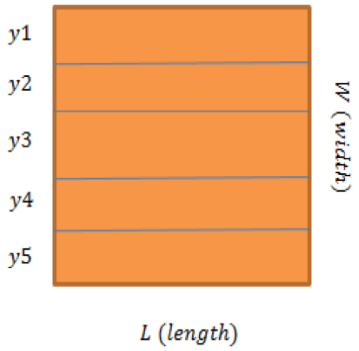

Figure 26: *Microstrip patch antenna meshing grid in ADS MoM solver*

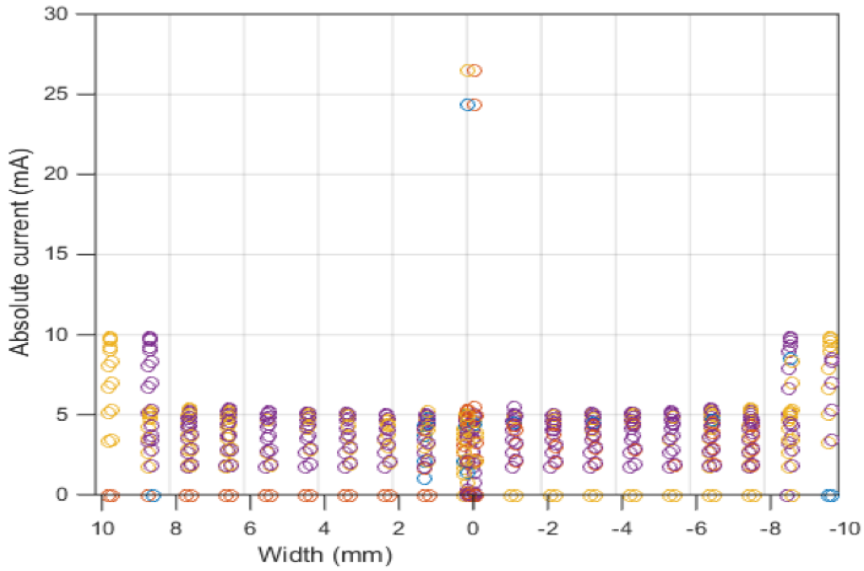

Figure 27: *Microstrip patch antenna surface current along its width from ADS MoM solver*

In Table 3, the poles required to reconstruct the patch antenna surface current are shown, where each cell requires two poles to form the whole 2D ACGF of the patch. Moreover, Figure 28 shows the complex poles representation for each cell as well as the initial reconstruction (first attempt; solving the problem in 2D) as shown in Figure 29.

Table 3: *SEM spatial poles representation of microstrip patch antenna cells*

Poles	**First cell (y1)**	**Second cell (y2)**	**Third cell (y3)**	**Fourth cell (y4)**	**Fifth cell (y5)**
s_1	$-0.00346 + j190.88$	$0.3180 + j189.904$	$-3.3804 + j173.945$	$0.3180 + j189.904$	$-0.00346 + j190.88$
s_2	$-0.00346 - j190.88$	$0.3180 - j189.904$	$-3.3804 - j173.945$	$0.3180 - j189.904$	$-0.00346 - j190.88$

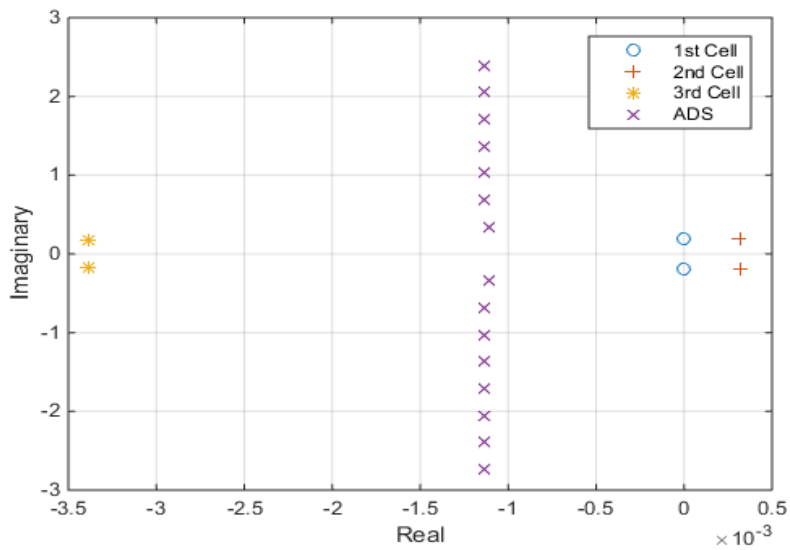

Figure 28: *SEM spatial poles representations of microstrip patch antenna, the optimized poles are represented as "X" while the approximated approach is showing TWO poles on each cell*

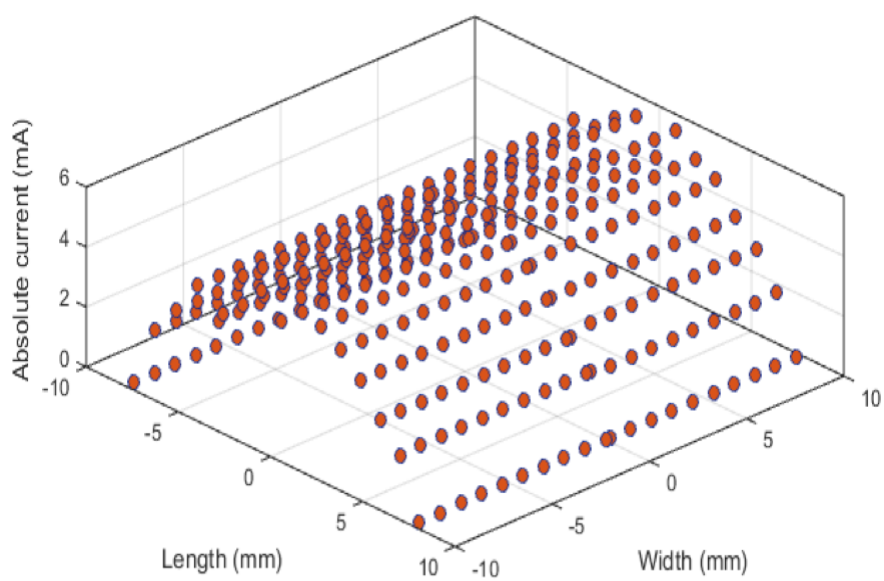

Figure 29: *Microstrip patch antenna reconstructed surface current given from optimizing the SEM poles and residues*

4 Helix antenna

In this section we introduce a complex EM structure, Helix, with dimensions as shown in Figure 30 that operates in frequencies range between 1 to 2 GHz as shown in Figure 31. It is required to obtain the SEM complex poles representation of the system in time domain using CST-MWS and also in spatial-frequency domain using CST-MWS. In RCS setup, the antenna is shorted or loaded and a plane wave is applied toward the target as shown in Figure 35, where the electric field component is tangential to the helix in the x-direction. The dependant frequency RCS is also plotted as shown in Figure 32

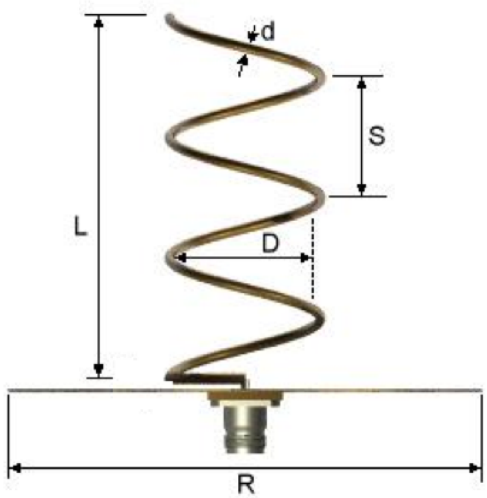

Figure 30: *Helix antenna and dimensions*

Table 4: *Helix antenna design dimensions*

Coil height (L)	$207mm$
Coil radius (D/2)	$34.3mm$
Number of turn	9
Wire radius (d/2)	$0.6mm$
Ground radius (R/2)	$100mm$
Turns separation (S)	$22.2mm$

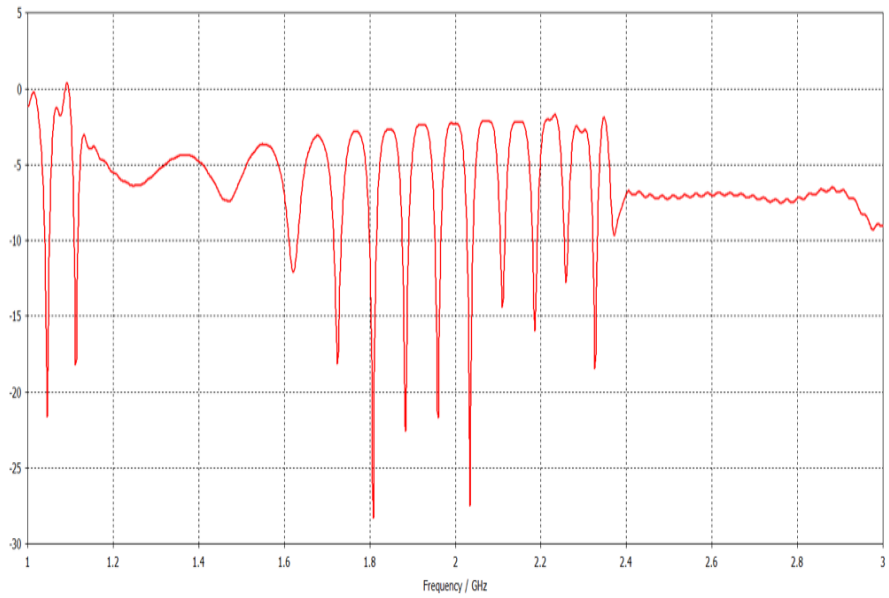

Figure 31: *Return loss in (dB) of Helix antenna operating between 1.6 to 2.4 GHz*

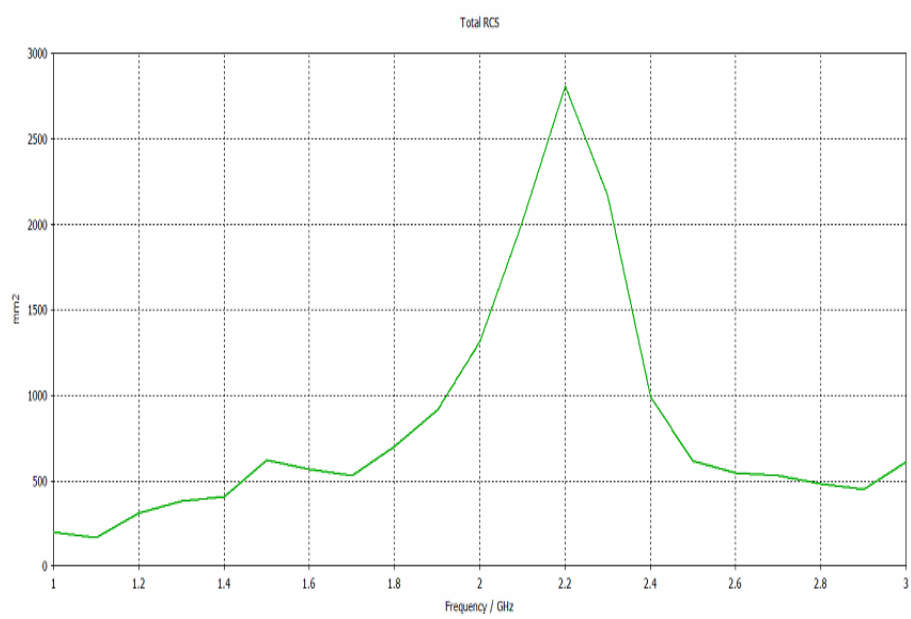

Figure 32: *Helix antenna frequency dependent RCS*

The 3D far field pattern of the helix is plotted as in Figures 33 and 34 that show the normal (broadside) and axial (end-fire) modes, respectively.

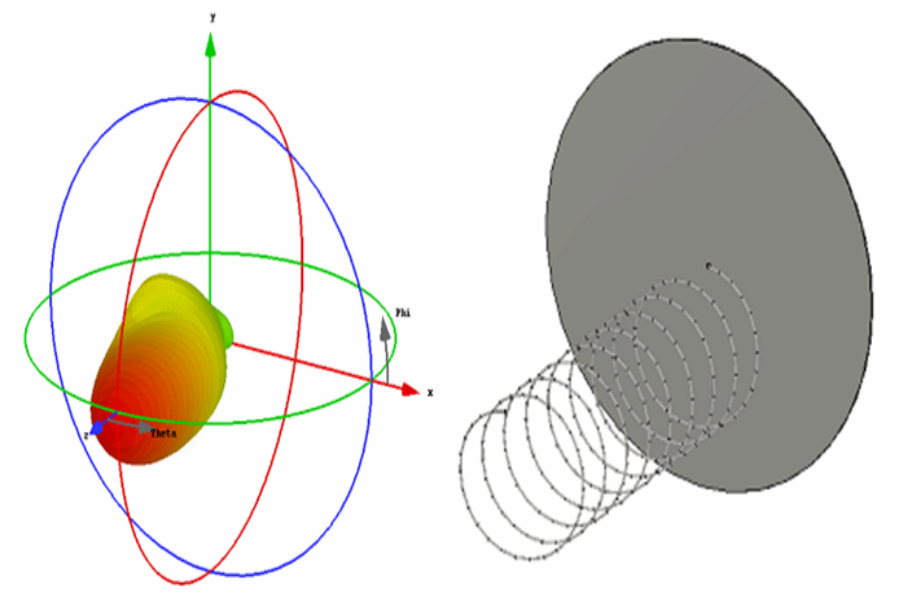

Figure 33: *Helix antenna radiation pattern in normal mode (Broadside); 3D representation*

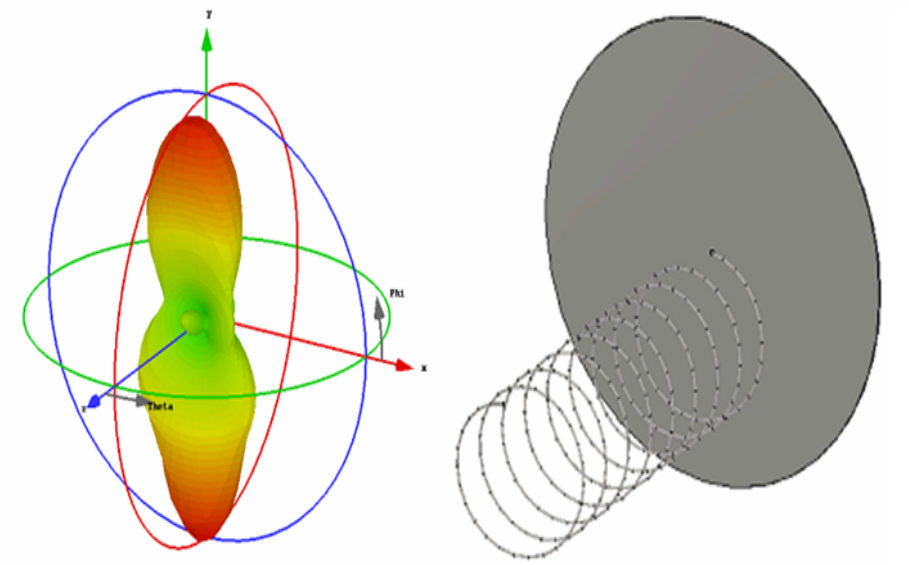

Figure 34: *Helix antenna radiation pattern in axial mode (end-fire); 3D representation*

4.1 Time domain SEM approach

As in the previous examples, the time domain simulation assumes a unit-impulse plane wave applied towards the antenna, while also a field probe is placed between the plane wave and the element to capture the scattered fields. The returned field is plotted in the z-direction showing the early time response as in Figure 36. In Figure 37, the late time field is plotted in comparison with SEM fitted fields by Prony's method, in which both fields are in close agreement to each other. The SEM complex poles representation is plotted in Figure 38 showing seven poles required to reconstruct the late time field.

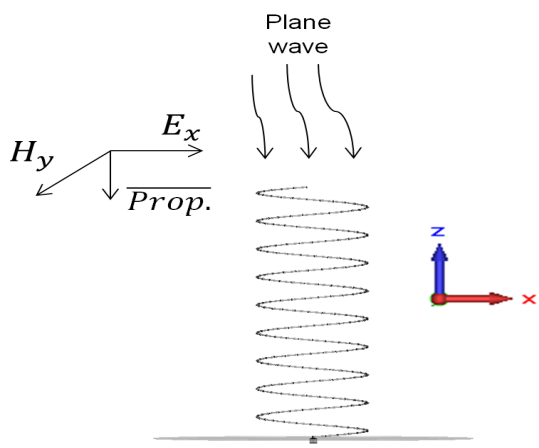

Figure 35: *Plane wave excitation of Helix in scattering mode between 1 to 2.4 GHz.*

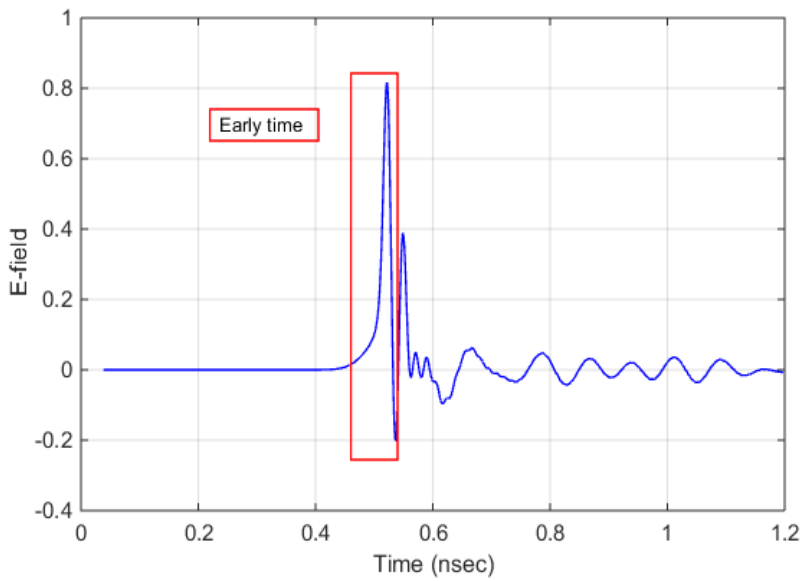

Figure 36: *Time domain electric field in z-direction of Helix in scattering mode between 1 to 2.4 GHz.*

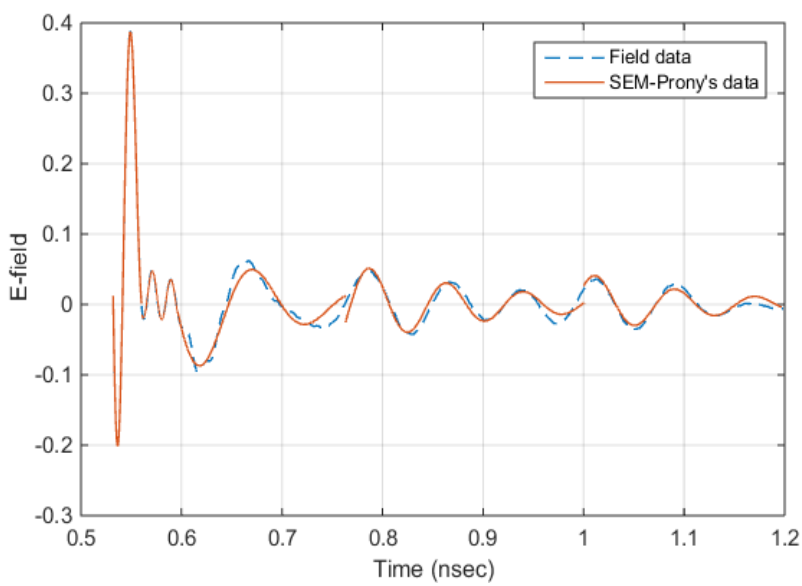

Figure 37: *SEM fitting of time domain field in z-direction of Helix in scattering mode.*

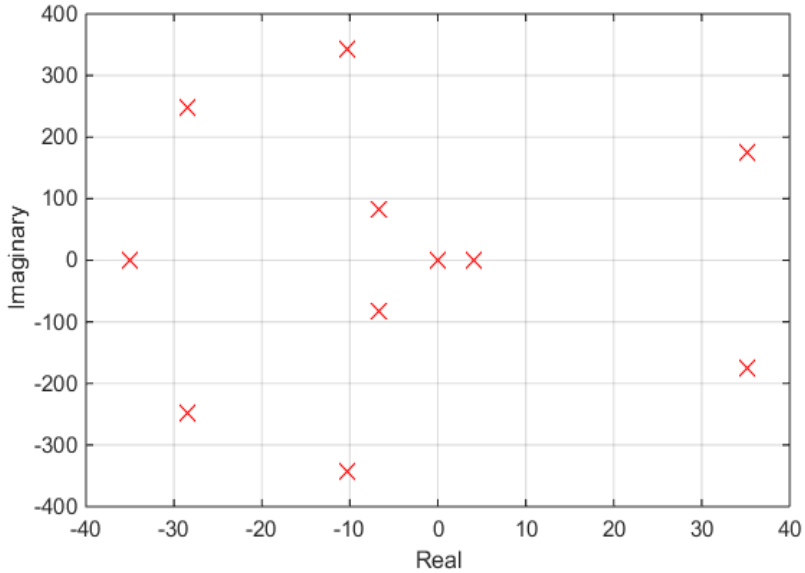

Figure 38: *SEM complex poles representation of Helix in scattering mode.*

4.2 Spatial-frequency ACGF-SEM approach

As in the previous examples, we assume the antenna in transmitting mode, where a unit-delta excitation signal is assumed in a fixed point in order to generate the antenna transfer function ACGF. In Figure 39, the current distribution is plotted in 3D on the antenna surface using CST-MWS. It shows a complex and random perturbations of the current, which can be observed in Figure 40, due to the FDTD meshing size and resolution on the antenna. However, the presented data are preliminary results for our next phase to deploy the system on MoM EM solvers. As modeling 3D geometries in MoM solvers are challenging and complex in terms of calculation time.

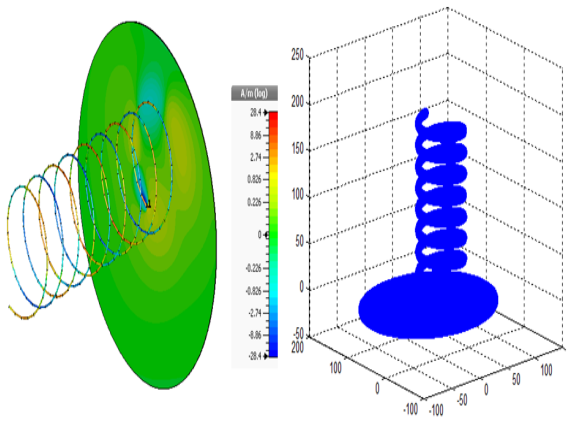

Figure 39: *Helix antenna current distribution; 3D representation*

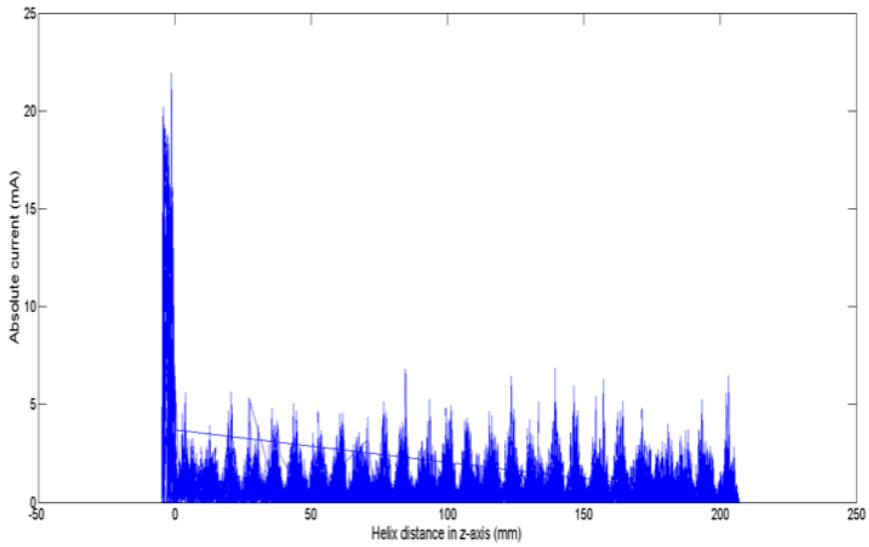

Figure 40: *Helix antenna current distribution; 2D representation*

In Figure 41, the CST-MWS surface current points have been reduced in order to obtain the SEM characterization. Using Prony's method, an accepted approximation has been made to fit the surface current perturbations using thirteen complex poles as shown in Figure 42.

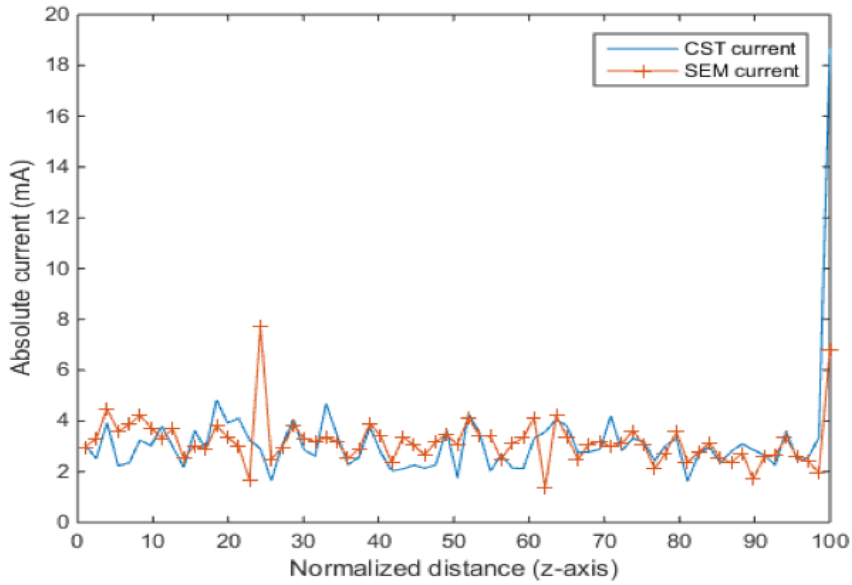

Figure 41: *ACGF Vs ACGF-SEM of helix antenna*

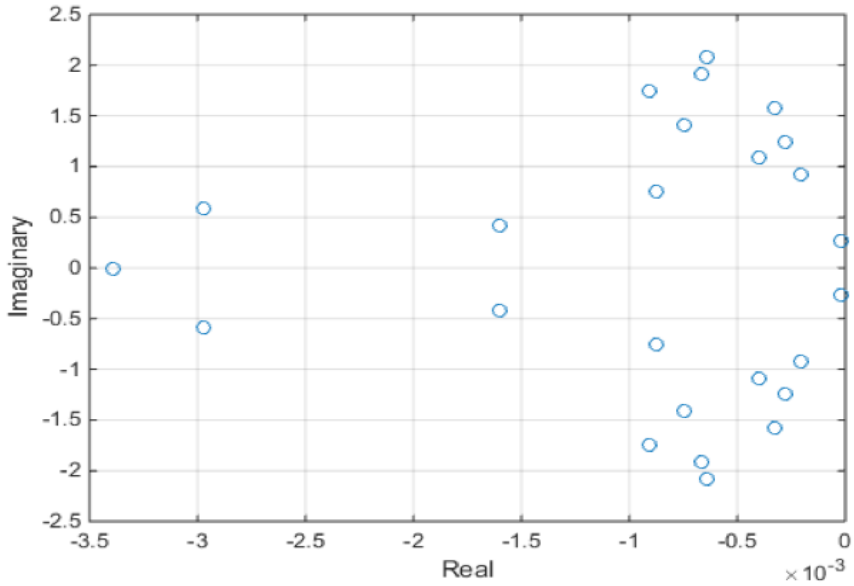

Figure 42: *SEM poles representation of helix antenna*

5 Conclusion

We presented a general formulation of the Singularity Expansion Method (SEM) applied to electromagnetic signals via the Antenna Current Green's Function (ACGF) in comparison to the conventional temporal formulation. The resulting ACGF-SEM theory was extended to include the far-field and exact analytical expression of the radiation pattern in terms of SEM data was found, leading to the discovery of RCS of targets [16]. The algorithm is applied successfully to some numerical examples involving wire antennas by representing target's unique signature. It is also expanded to Microstrip patch antennas (a form of planar structures) which is illustrated throughout this work. The form of a complex wire (merging magnetic and electric dipoles together), helix, is also presented and discussed to fortify our theory. Our aim is to establish a rigorous ACGF-SEM mathematical model on arbitrary antenna shapes and represent a spatial-frequency features instead of the temporal fields. In the future, the ACGF-SEM-RCS theory will be expanded over arbitrary antenna shapes, which will be the precursor in exploring new modelling schemes for RCS of targets.

Annex A: MATLAB codes

```
% ACGF-SEM for thin-wire antenna

clc
close all
clear all
tic
result = [];
M=[1];
[~ , B , ~]=textread(['C:\Users\alzaheda\Dropbox\WIPL-D Project\',num2str(M),'dipole.cu1'],'%s%s%s'); % Importing the antenna surface current
N=str2double(B(4)); % Mesh points
f=str2double(B(3))*1e9; % Operating frequency 30e9

[~ , B1 , C1]=textread(['C:\Users\alzaheda\Dropbox\WIPL-D Project\',num2str(M),'dipole.shw'],'%f%f%f'); % Importing antenna data
l=C1(7);
numberOfele=B1(3);
fid=fopen(['C:\Users\alzaheda\Dropbox\WIPL-D Project\',num2str(M),'dipole.cu1']);
while 1
    tline = fgetl(fid);
    if ~ischar(tline), break, end
    celldata = textscan(tline,'%f %f %f ');
    matdata = cell2mat(celldata);
    result = [result ; matdata];
end
fclose(fid);

IR=result(:,2);
IM=result(:,3);
I=(IR+1i*IM);

II=reshape(I,[],0.25*numberOfele^2); % Rshape the matrix for multiple elements

S=linspace(l,-l,2*N); % total antenna length
c=3e8;
lambda=c/f;
```

```
betao=2*pi/lambda;
theta=linspace(0,90,N);
p=2; % number of SEM poles

%%%%%%%%%%%%%%%%%%%%%%%%%%%%%%%%%%%%
%% ACGF-SEM through PronyŠs method

for k=1:(numberOfele/2)*M
    [b(:,k),R(:,k)]=mprony(II(:,k),S,p);
End

dl=S(2)-S(1); % step
ttt=[];
t=1:N;

%%%%%%%%%%%%%%%%%%%%%%%%%%
%% Plane wave definition

pw_theta=(270-theta)*pi/180;
pw_phi=zeros(size(pw_theta))*pi/180;
pw_mag_theta=1;
pw_mag_phi=0;

r_x = 0 ;
r_y = 0 ;
r_z = S ;

pw_SphMat = [
     0                ;
     pw_mag_theta     ;
     pw_mag_phi ]     ;

% matrix to convert spherical to cartesian
MatEntry11 = (sin(pw_theta).*cos(pw_phi))';
MatEntry12 = (cos(pw_theta).*cos(pw_phi))';
MatEntry13 = (-sin(pw_theta).*sin(pw_phi))';

MatEntry21 = (sin(pw_theta).* sin(pw_phi))';
MatEntry22 = (cos(pw_theta).* sin(pw_phi))';
MatEntry23 = (sin(pw_theta).* cos(pw_phi))';

MatEntry31 = (cos(pw_theta))';
```

```
MatEntry32 = (-sin(pw_theta))';
MatEntry33 = 0;

OutputMatrix      = zeros(3,3,N);

OutputMatrix(1,1,:) = MatEntry11;
OutputMatrix(1,2,:) = MatEntry12;
OutputMatrix(1,3,:) = MatEntry13;


OutputMatrix(2,1,:) = MatEntry21;
OutputMatrix(2,2,:) = MatEntry22;
OutputMatrix(2,3,:) = MatEntry23;

OutputMatrix(3,1,:) = MatEntry31;
OutputMatrix(3,2,:) = MatEntry32;
OutputMatrix(3,3,:) = MatEntry33;

Sph2CartMat = OutputMatrix;
Sph2CartMatd = permute(Sph2CartMat,[1 3 2]);
Sph2CartMatd = reshape(Sph2CartMatd,[],size(Sph2CartMat,2),1)
    ;
pw_CartMat  =  Sph2CartMatd * pw_SphMat      ;
pw_CartMat=reshape(pw_CartMat,3,1,100);

k_x = -betao * sin(pw_theta).* cos(pw_phi) ;
k_y = -betao * sin(pw_theta).* sin(pw_phi) ;
k_z = -betao * cos(pw_theta)' ;
k_z=reshape(k_z,1,1,100);
% compute the received field


E = bsxfun(@times, pw_CartMat, exp( 1i * bsxfun(@times, k_z,
    r_z) ) ) ;
E = permute(E,[2 1 3]) ;

%%%%%%%%%%%%%%%%%%%%%%%%%%%%%%
iii=zeros(length(theta),1);
for t=1:100
for k=1:(numberOfele/2)*M
            ii(k,t)=0;

```

```
        for n=1:p
                ii(k,t)=ii(k,t)+R(n,k)*exp(b(n,k)*S)*E(:,3,t)*dl; % Port currents at different angles given SEM poles

         end

end
iii(t)=iii(t)+II'*E(:,3,t)*dl; % Received current at different angles given ACGF
end
%%%
```

```
toc
```

```
%% Processing the surface current of thin-wire antenna to find the radiated
%% field through ACGF-SEM modeling (RCS-ACGF-SEM)
clc
close all
clear all
tic
result = [];
M=[1];
[~ , B , ~]=textread(['C:\Users\alzaheda\Dropbox\WIPL-D Project\RCS\',num2str(M),'dipole.cu1'],'%s%s%s'); % Reading the surface current from % WIPL-D
N=str2double(B(4)); % number of meshing points defined in WIPL-D
f=str2double(B(3))*1e9; % operating frequency 30e9
% extract the antenna length divided by 2
[~ , B1 , C1]=textread(['C:\Users\alzaheda\Dropbox\WIPL-D Project\RCS\',num2str(M),'dipole.shw'],'%f%f%f'); % reading dipole antenna data
l=C1(9); % antenna length/2
numberOfele=B1(3); % the dipole antenna is defined as two elements connected to each other
%%%%%%%%%%%%%%%%%%%%%%%%%%%%%%%%%%%%
%% Refining the input data by excluding any characters from the file

fid=fopen(['C:\Users\alzaheda\Dropbox\WIPL-D Project\RCS\',num2str(M),'dipole.cu1']);
while 1
    tline = fgetl(fid);
    if ~ischar(tline), break, end
    celldata = textscan(tline,'%f %f %f ');
    matdata = cell2mat(celldata);
    result = [result ; matdata];
end
fclose(fid);

%%%%%%%%%%%%%%%%%%%%%%%%%%%%%%%%%%%%

```

```
IR=result(:,2); % Real surface current
IM=result(:,3); % Imaginary surface current
I=(IR+1i*IM)*1e-3; % Combining the real and imag currents in mA
II=reshape(I,[],0.25*numberOfele^2); % Reshape the matrix to multiple columns elements
S=linspace(-l,l,2*N); % full antenna length with 2N meshing points
c=3e8; % Speed of light
lambda=c/f; % wavelength
betao=2*pi/lambda; % Propagation number
theta=linspace(-180,180,N); % Elevation angle scanning
 p=3; % number of SEM poles
%%%%%%%%%%%%%%%%%%%%%%%%%%%%%%%%%%%%
%% PronyŠs method to calculate SEM poles (b) and Residues (R)
for k=1:(numberOfele/2)*M
    [b(:,k),R(:,k)]=mprony(II(:,k),S,p);
End
%%%%%%%%%%%%%%%%%%%%%%%%%%%%%%%%%%%%
%% Plane wave data

pw_theta=(theta)*pi/180;
pw_phi=zeros(size(pw_theta))*pi/180;
k_x = (cos(pw_theta) .* cos(pw_phi))' ;
k_y = (cos(pw_theta) .* sin(pw_phi))' ;
k_z = sin(pw_theta)' ;

%%%%%%%%%%%%%%%%%%%%%%%%%%%%%%%%%%%%
%% Defining the ACGF-SEM formula in equation (6)

LL=[0 0 1]'; % Antenna is orientated on the z-axis
k=[];
for ij=1:N
k(ij,:)=[k_x(ij)  k_y(ij)  k_z(ij)];
Dyad(:,:,ij)=eye(length(k(ij,:)))-(k(ij,:)'*k(ij,:)); % defining the Dyadic function
end

fn=[];
for n=1:p
    for mn=1:N
fn(mn,n)= ( exp( ( 1i*betao*k(mn,:)*LL + b(n) )*l ) - exp(
```

```
    (-1i*betao*k(mn,:)*LL - b(n) )*l ) )  / ( 1i*betao*k(mn,:)
    *LL + b(n)) ;
      fnr(mn,n)=(R(n)) * fn(mn,n);
      end
end

fns = sum(fnr,2); % The vslur of fn function in equation (7)


for nn=1:N
      Etotal(nn,:) =  fns(nn,:) * Dyad(:,:,nn) * LL  ; % Field
         from ACGF-SEM
      Eold(nn,:) = II(nn,:) * Dyad(:,:,nn) * LL *exp(1i*betao*
         k_z(nn)); % Field from ACGF function only (II)

end

%%%%%%%%%%%%%%%%%%%%%%%%%%%%%%%%
Data=importdata('C:\Users\alzaheda\Dropbox\WIPL-D Project\RCS
    \field.txt');% Reading the field given from the WIPL-D
thetaWIPL=Data(:,1)*pi/180;
Eabs=(Data(:,2))/max((Data(:,2))); % WIPL_D gain
Etotalabs=abs(Etotal(:,3)) /max(abs(Etotal(:,3))); % ACGF-SEM
     field

Error=(1/N)*sum(abs(Eabs-Etotalabs).^2)

polar(thetaWIPL,Eabs)
hold on
polar(pw_theta',Etotalabs,'r--')
legend('WIPL-D field','ACGF-SEM field')
grid on
toc
```

```
%% Fitting the ACGF on the patch surface to a sinusoidal
    function

x=linspace(-7.74,7.74,1212); % Patch length

%%%%%%%%%%%%%%%%%%%%%%%%%%%%%%%%%%%%%%%%%%
%% First cell as mentioned in the Patch antenna section

```

```
xc1=-8.22988;
w1=16.45779;
A1=10.01851;
y01=0;
y1=y01+A1*sin(pi*(x-xc1)/w1);

%% Second cell as mentioned in the Patch antenna section

xc2=-332.56866;
w2=665.0943;
A2=7373.54451;
y02=-7368.31118;
y2=y02+A2*sin(pi*(x-xc2)/w2);

%% Third cell as mentioned in the Patch antenna section

xc3=1208.30153;
w3=805.40116;
A3=7519.86735;
y03=-7515.62163;
y3=y03+A3*sin(pi*(x-xc3)/w3);

%%%
```

```
II1(m)=sum1;
II2(m)=sum2;
II3(m)=sum3;

end

bx=importdata('poles.mat'); % EM solver extracted poles
scatter(real(b1),imag(b1))
hold on
scatter(real(b2),imag(b2),'+')
hold on
scatter(real(b3),imag(b3),'*')
grid on
xlabel('Real') % x-axis label
ylabel('Imaginary') % y-axis label
box on
legend('1st Cell','2nd Cell','3rd Cell')
```

```
% Helix antenna ACGF-SEM modeling

clc
clear

[x,y,z,x_real,y_real,z_real,x_imag,y_imag,z_imag,~] =
    textread( 'C:\Users\alzaheda\Desktop\helix.txt' , '%f%f%f%
    f%f%f%f%f%f%f',61038, 'headerlines', 2); % Importing
    Helix antenna surface current
x_current=x_real+1i*x_imag;
y_current=y_real+1i*y_imag;
z_current1=z_real+1i*z_imag;

z_current=unique(abs(z_current1),'stable');

I=(unique(z_real+1i*z_imag,'stable')); % Total Current from
    WIPL-D (z-axis)
I=smooth(I,'moving');
I=abs(I);
p=25; % number of SEM poles
LL=findpeaks(I); % sorting the current to be easily plotted
LL=findpeaks(LL);
LL=findpeaks(LL);
LL=findpeaks(LL);
```

```
SL=linspace(1,100,length(LL))'; % Helix antenna normalized length on z-axis

%% Defining the SEM poles and residues through PronyŠs method

[b, R]=mprony(LL,SL,p);

for m=1:length(SL)
    sum=0;
for n=1:p
    sum=sum+R(n)*exp(b(n)*SL(m));
end
II1(m)=sum;
end
figure(1)
% title('Helix current distribution after smoothing Vs SEM reconstruction')
plot(SL,(LL),SL,abs(II1),'+-');
xlabel('Normalized distance (z-axis)') % x-axis label
ylabel('Absolute current (mA)') % y-axis label
legend('CST current','SEM current')

scatter(real(b),imag(b))
grid on
box on
xlabel('Real')
ylabel('Imaginary')
```

References

[1] C. A. Balanis, Antenna Theory: Analysis and Design, 2nd ed. Hoboken, NJ, USA: Wiley, 1997.

[2] C. Baum, "Emerging technology for transient and broadband analysis and synthesis of antennas and scatterers," *Proceedings of the IEEE*, vol. 64, pp. 1598-1616, 1976.

[3] C. Baum and E. Rothwell, "The singularity expansion method and its application to target identification," *Proceedings of the IEEE*, vol. 79, pp. 1481-1492, October 1991.

[4] C. Baum, *The Singularity Expansion Method In Electromagnetics: A Summary Survey And Open Questions*, Lulu Enterprises, Inc, 2012.

[5] S. M. Mikki and Y. M. M. Antar, "The Antenna Current Green's Function Formalism—Part I," *IEEE Trans. Antennas Propagat.*, no. 9, vol. 61, pp. 4493–4504, September 2013.

[6] S. M. Mikki and Y. M. M. Antar, "The Antenna Current Green's Function Formalism—Part II," *IEEE Trans. Antennas Propagat.*, no. 9, vol. 61, pp. 4505-4519, September 2013.

[7] S. M. Mikki, Y. M. Antar, New Foundations for Applied Electromagnetics: The Spatial Structure of Fields, Artech House, Norwood, MA 02062 USA, 2016.

[8] Branko Kolundzija and Antonije Djordjevic, *Electromagnetic Modeling of Composite Mettallic and Dielectric Structures*, Artech House, 2002.

[9] S. A. Schelkunoff,"A Mathematical Theory of Linear Arrays," *Bell System Technical Journal*, Vol. 22, pp. 80–107, 1943.

[10] A. G. Ramm, "Mathematical foundations of the singularity and eigenmode expansion methods," *Journal of Mathematical Analysis and Applications*, no. 86, pp. 562–591, 1982.

[11] L. V. Blake, Radar Range Performance Analysis, Artech House, ISBN 0-89006-224-2, Norwood, USA, 1986.

[12] CST-MWS, EM solver, 2015.

[13] WIPL-D, EM solver, Ver. 9.

[14] A. M. Alzahed, S. M. Mikki and Y. M. Antar, "Characterization of A Rectangular Patch Antenna Using ACGF-SEM Approach," *IEEE Conference on Antenna Measurements and Applications (CAMA)*, Syracuse, USA, 2016.

[15] ADS, EM solver, 2015.

[16] A. M. Alzahed, S. M. Mikki, Y. M. M. Antar, M. Clenet and S. Jovic, "The ACGF-SEM Approach To Electromagnetic Radiation With Applications In Radar And Inverse Modeling," *International Union of Radio Science URSI*, 2017, Montreal.

DOCUMENT CONTROL DATA

*Security markings for the title, authors, abstract and keywords must be entered when the document is sensitive

1. ORIGINATOR (Name and address of the organization preparing the document. A DRDC Centre sponsoring a contractor's report, or a tasking agency, is entered in Section 8.) Royal Military College of Canada P.O. Box 17000, Stn. Forces, Kingston, ON K7K 7B4	2a. SECURITY MARKING (Overall security marking of the document, including supplemental markings if applicable.) CAN UNCLASSIFIED 2b. CONTROLLED GOODS NON-CONTROLLED GOODS DMC A

3. TITLE (The document title and sub-title as indicated on the title page.)

Antenna RCS Characterization using SEM approach

4. AUTHORS (Last name, followed by initials – ranks, titles, etc. not to be used. Use semi-colon as delimiter)

Alzahed, A. M.; Mikki, S. M.; Antar, Y. M. M.

5. DATE OF PUBLICATION (Month and year of publication of document.)	6a. NO. OF PAGES (Total pages, including Annexes, excluding DCD, covering and verso pages.)	6b. NO. OF REFS (Total cited in document.)
October 2018	44	16

7. DOCUMENT CATEGORY (e.g., Scientific Report, Contract Report, Scientific Letter)

Contract Report

8. SPONSORING CENTRE (The name and address of the department project or laboratory sponsoring the research and development.)

DRDC – Ottawa Research Centre
3701 Carling Avenue, Ottawa ON K1A 0Z4, Canada

9a. PROJECT OR GRANT NO. (If appropriate, the applicable research and development project or grant number under which the document was written. Please specify whether project or grant.)	9b. CONTRACT NO. (If appropriate, the applicable contract number under which the document was written.) SLA RMCC-DRDC Serial #2014-007-SLA, Annex #PA14006 - SEM Development for Antenna Characterization
10a. DRDC DOCUMENT NUMBER DRDC-RDDC-2017-C335	10b. OTHER DOCUMENT NO(s). (Any other numbers which may be assigned this document either by the originator or by the sponsor.)

11a. FUTURE DISTRIBUTION WITHIN CANADA (Approval for further dissemination of the document. Security classification must also be considered.)

Public release

11b. FUTURE DISTRIBUTION OUTSIDE CANADA (Approval for further dissemination of the document. Security classification must also be considered.)

Public release

12. KEYWORDS, DESCRIPTORS or IDENTIFIERS (Use semi-colon as a delimiter.)

Antenna Characterization; RCS; Singular Expansion Method

13. ABSTRACT/RÉSUMÉ (When available in the document, the French version of the abstract must be included here.)

The report investigates antenna characterization using the singularity expansion method (SEM) in both time and spatial-frequency domains. The motivation is to obtain the radar cross section (RCS) of targets through newly and eficient methods. The in-vestigation covers three target types; dipole (thin-wire), u-strip patch and helical antennas. Each target's features are determined using the temporal SEM approach and also by the newly developed approach antenna current Green's function (ACGF) in spatial-frequency domain. The temporal SEM works by inspecting the time domain field representation within a specific time window. In contrast, the ACGF approach is applied on the targets characteristic current (surface current due to special excitation). Both methods are applied on the three mentioned targets to validate the concept.

Le rapport étudie la caractérisation d'antenne en utilisant la méthode d'expansion de la singularité (SEM) dans les domaines temporels et spatiotemporels. La motivation est d'obtenir la section efficace du radar (RCS) des cibles grace a des méthodes nouvelles et efficaces. L'enquete couvre trois types de cibles; dipole (fil mince), patch en U et antennes hélicoidales. Les caractéristiques de chaque cible sont déterminées a l'aide de l'approche temporelle SEM et aussi par la fonction de Green de l'antenne d'approche nouvellement développée (ACGF) dans le domaine spatial-fréquence. Le SEM temporel fonctionne en inspectant la représentation du champ du domaine temporel dans une fenetre temporelle spécifique. En revanche, l'approche ACGF est appliquée sur le courant caractéristique des cibles (courant de surface du a une excitation spéciale). Les deux méthodes sont appliquées sur les trois cibles mentionnées pour valider le concept.